

**IMPROVED DATA COMPRESSION TECHNIQUES TO
ANALYZE BIG DATA IN STRUCTURAL HEALTH
MONITORING**

by

Nawaf Hussain Almasri

A thesis

submitted to the Faculty of Graduate Studies

in partial fulfilment of the requirement for the

degree of Master of Science

in

Civil Engineering

Lakehead University

Thunder Bay, Ontario

May 2018

Dedicated to my family

Table of Contents

List of Tables	v
List of Figures	xi
Abstract	xii
Acknowledgements	xiv
Chapter 1 Introduction	1
1.1 Structural Health Monitoring	1
1.2 Modern Sensing and Big Data	3
1.3 Data Compression Techniques	5
1.4 Literature Review of Data Compression Methods	6
1.5 Gap Areas	12
1.6 Thesis Objectives	13
Chapter 2 Proposed Method	15
2.1 L_1 -norm Minimization	15
2.2 Discrete Cosine Transform	17
2.3 Time-Frequency Blind Source Separation	23
2.4 Proposed Methodology	26
Chapter 3 Validation of Wireless Sensor Network	28
3.1 Background	28
3.1.1 Narada	28
3.1.2 Other Sensing Devices	29

3.2	Experimental Validation	31
Chapter 4	Numerical Studies	35
4.1	4-DOF Model	35
4.2	10-DOF Model	41
Chapter 5	Experimental and Full-scale Validation	48
5.1	Model A	48
5.1.1	Explicit Data Compression	49
5.1.2	Implicit Data Compression	53
5.2	Model B	56
5.2.1	Baseline (w/o any damage)	57
5.2.2	Effect of Discrete Damage	64
5.3	Cantilever Beam	71
5.4	Full-scale Study	75
Chapter 6	Conclusions and Future Work	82
6.1	Key Conclusions	82
6.2	Achievements	83
6.3	Future Work	83
6.4	Acronyms	84
Bibliography	86
A	Implementation of Narada Sensors	90

List of Tables

3.1	Summary of frequency analysis obtained from three different sensors under a wide range of excitation	34
4.1	Size of the norm of the original and reconstructed data by DCT	40
4.2	Identification results of the 10-DOF model using DCT method	47
5.1	Details of implicit data compression	54
5.2	Summary of TFBSS results obtained from the original and reconstructed data by DCT for undamaged and damaged tests .	70
5.3	Identification results using the original and reconstructed data by LNM and DCT	81
6.1	List of acronyms	85

List of Figures

1.1	Wireless sensing unit of (a) Imote2 and (b) Narada [7]	4
1.2	Formation of big data in modern sensing network and their potential challenges	5
2.1	Flowchart of the DCT [30]	20
2.2	The performance of DCT method in data compression	22
2.3	Flowchart of the implementation of DCT	23
2.4	(a) Time history and (b) Fourier spectra of the mixture of sine signals	25
2.5	(a) Time history and (b) Fourier spectra of modal responses obtained from the TFBSS	26
2.6	Flowchart of the proposed method	27
3.1	Narada WSN: (a) one sensing transducer attached to a Narada unit, (b) base station attached to a laptop	29
3.2	(a) Trigno and (b) high speed camera obtained from the Department of Kinesiology at Lakehead University	30
3.3	Narada, Trigno and Camera attached to the experimental model	31
3.4	Time histories of floor responses measured by (a) Narada, (b) Trigno and (c) camera obtained from the impact force test . .	32
3.5	Fourier spectra of floor responses measured by (a) Narada, (b) Trigno and (c) camera obtained from the impact force test . .	33
3.6	Time history of floor responses measured by (a) Narada, (b) Trigno and (c) camera obtained from the random force test . .	33

3.7	Fourier spectra of floor responses measured by (a) Narada, (b) Trigno and (c) camera obtained from the random force test . . .	34
4.1	4-DOF Model	35
4.2	Time histories of floor responses obtained from the 4-DOF model	36
4.3	20% data compression of first floor response by LNM	37
4.4	50% data compression of first floor response by LNM	37
4.5	20% data compression of fourth floor response by LNM	38
4.6	50% data compression of fourth floor response by LNM	38
4.7	(a) Time histories and (b) Fourier spectrum of floor responses obtained from reconstructed data using DCT	39
4.8	Convex hull of the data norm: (a) original data and (b) reconstructed data	40
4.9	10-DOF Model	41
4.10	Time histories of floor responses obtained from the 10-DOF model	42
4.11	Fourier spectra of floor responses obtained from the 10-DOF model	42
4.12	Fourier spectra of modal responses obtained from TFBSS using the original data	43
4.13	Time histories of floor responses obtained from the reconstructed data by LNM	44
4.14	Fourier spectra of floor responses obtained from the reconstructed data by LNM	44
4.15	Fourier spectra of modal responses obtained from TFBSS using the reconstructed data by LNM	45

4.16	Time histories of floor responses obtained from the reconstructed data by DCT	46
4.17	Fourier spectra of floor responses obtained from the reconstructed data by DCT	46
4.18	Fourier spectra of modal responses obtained from TFBSS using the reconstructed data by DCT	47
5.1	Model A	49
5.2	20% data compression of third floor by LNM	50
5.3	40% data compression of third floor by LNM	50
5.4	60% data compression of third floor by LNM	51
5.5	Time histories of floor responses obtained from (a) original data, (b) reconstructed data by LNM and (c) reconstructed data by DCT	52
5.6	Fourier spectra of floor responses obtained from (a) original data, (b) reconstructed data by LNM and (c) reconstructed data by DCT	52
5.7	Fourier spectra of modal responses using TFBSS obtained from (a) original data, (b) reconstructed data by LNM and (c) reconstructed data by DCT	53
5.8	(a) Time history of Test 1, (b) Fourier spectrum of Test 2, (c) Time history of the reconstructed signal of Test 1 by LNM, and (d) Fourier spectrum of reconstructed signal of Test 1 by LNM	54
5.9	Fourier spectrum of floor responses obtained from Test 1 using DCT	55
5.10	Model B	56
5.11	Location of six accelerometers placed on Model B	57

5.12	Time history of floor responses obtained from Model B before damage (white noise)	58
5.13	Fourier spectrum of floor responses obtained from Model B before damage (white noise)	59
5.14	Time history of floor responses obtained from Model B before damage (ground motions)	59
5.15	Fourier spectrum of floor responses obtained from Model B before damage (ground motions)	60
5.16	Time history of floor responses obtained from the reconstructed data by DCT (white noise)	60
5.17	Fourier spectrum of floor responses obtained from the reconstructed data by DCT (white noise)	61
5.18	Time history of floor responses obtained from the reconstructed data by DCT (ground motions)	61
5.19	Fourier spectrum of floor responses obtained from the reconstructed data by DCT (ground motions)	62
5.20	Fourier spectra of modal responses using TFBSS obtained from (a) original data and (b) reconstructed data by DCT	63
5.21	Damage occurs on first level of Model B due to loosening of bolt	64
5.22	Time history of floor responses obtained from Model B after damage (white noise)	65
5.23	Fourier spectrum of floor responses obtained from Model B after damage (white noise)	65
5.24	Time history of floor responses obtained from Model B after damage (ground motions)	66
5.25	Fourier spectrum of floor responses obtained from Model B after damage (ground motions)	66

5.26	Time history of floor responses obtained from the reconstructed data by DCT (white noise)	67
5.27	Fourier spectrum of floor responses obtained from the reconstructed data by DCT (white noise)	67
5.28	Time history of floor responses obtained from the reconstructed data by DCT (ground motions)	68
5.29	Fourier spectrum of floor responses obtained from the reconstructed data by DCT (ground motions)	68
5.30	Fourier spectra of modal responses using TFBSS obtained from (a) original data and (b) reconstructed data by DCT	70
5.31	Cantilever beam attached with a shaker and accelerometers at IIT Kanpur	71
5.32	Time history of the beam responses under random base excitation	72
5.33	Fourier spectrum of the beam responses under random base excitation	72
5.34	Time history of the beam responses obtained from the reconstructed data	73
5.35	Fourier spectrum of the beam responses obtained from the reconstructed data	73
5.36	Fourier spectra of modal responses using TFBSS obtained from (a) original data and (b) reconstructed data by DCT	74
5.37	Long-span bridge in Thunder Bay	75
5.38	20% data compression by LNM	76
5.39	40% data compression by LNM	76
5.40	60% data compression by LNM	77
5.41	70% data compression by LNM	77

5.42	80% data compression by LNM	78
5.43	Accuracy of data reconstruction for all selected rates of compression	79
5.44	Compression by DCT with 10% threshold level	80
5.45	Fourier spectra of modal responses using TFBSS obtained from (a) original data, (b) reconstructed data by LNM and (c) reconstructed data by DCT	81
A1	Data acquisition system of Narada sensor	91

Abstract

With growing number of complex and slender structures worldwide, long-term structural health monitoring (SHM) has been intensively pursued to retrofit and control these structures under extreme climatic events. Modern sensing technology including wireless sensors and high quality data acquisitions have improved the capability of SHM where a relatively enormous amount of data could be measured remotely and sent wirelessly for a longer period of time. Unlike wired vibration sensors, wireless sensors are inexpensive and easier to install with less labour-intensive process, thereby leading to a significant cost-saving to the infrastructure owner. However, the modern sensing technology and remote data acquisition has some several limitations due to their limited bandwidth, time synchronization and inadequate sampling issues. The large amount of data collected from the structural systems often causes missing data, network jam or packet loss while transmitting the big data.

In this research, the theory of compressive sampling (CS) is implemented as a promising data compression technique that can recover undersampled vibration signals of dynamical systems, thereby reducing overall burden of analyzing big data in SHM. The l_1 -norm minimization (LNM) and discrete cosine transform (DCT) are exploited to perform data compression and enhance data recovery of the compressed big data. A novel time-frequency blind source separation is integrated with the data compression technique to evaluate the accuracy of the proposed method in modal identification. The results of the proposed data compression techniques are verified using a suite of numerical, experimental and full-scale studies. The results reveal that

DCT could be considered as a powerful data compression tool even for the vibration data containing damage signatures, low energy modes and low signal-to-noise ratio.

Acknowledgements

I would like to express my sincere thanks to Dr. Ayan Sadhu. I am honored and grateful to have him as my thesis supervisor. Dr. Sadhu has guided me with his critical thoughts, valuable support and great motivation to conduct my research.

I would like to thank to my committee members, Dr. Ehsan Rezazadeh Azar and Dr. Carlos Zerpa. Sincere thanks to Dr. Zerpa for his assistance with vision sensors for initial validation of wireless sensors. I would also like to express my gratitude to my research teammates (Mohamed Barbosh, Malek Lazhari, Chanakya Bodupalli, Peter Friesen and Sandeep Sony).

I thank Mitacs and Dr. Sadhu for providing the opportunity to engage in research collaboration overseas through *Mitacs Globallink Research Award*. With this award, I spent a term in Indian Institute of Technology (IIT) Kanpur in India and acquired valuable knowledge and research experience. Special thanks to Dr. Samit Ray Chaudhuri who assisted me to conduct several dynamic experiments with the world-class structural testing facility at IIT Kanpur. I also thank the City of Thunder Bay for providing access to the Main Street bridge for this research.

Sincere thanks and appreciations to the Saudi Arabian Cultural Bureau and The Ministry of Higher Education for their efforts to sponsor my graduate studies at Lakehead University in a continuous basis. I would like to express my sincere gratitude to my family for their continuous support and motivation to reach my goal and enrich my academic career. Many thanks to my brother (Mohammad) who has offered invaluable support and humor during my stay in Canada. Finally, I would like to

thank all of my amazing friends for making my journey spectacular.

Chapter 1

Introduction

In this chapter, a brief background of structural health monitoring (SHM) and its overall importance to monitoring large-scale infrastructure is first introduced. In SHM, structural condition assessment is undertaken based on a suite of rich measured vibration data using wired or wireless sensors. The importance of efficient data collection, acquisition and data transmission are emphasized within the framework of long-term monitoring of critical structures. Challenges of utilizing big data in SHM are explored and the potential limitations of existing wireless sensor network are discussed to develop gap areas of current research. Finally, specific objectives of this thesis are discussed.

1.1 Structural Health Monitoring

Civil engineering structures are primarily designed to withstand design loads and resist natural disasters or unusual excitation for a specific design life. These structures, however, continue to age with time and pose significant safety issues to the infrastructure owners. Extreme climatic events and adverse weather conditions in North America contribute further challenges in preventing progressive deterioration of these structures. In fact, as per the recent infrastructure report card of American Society of Civil Engineers (ASCE), the overall GPA of American infrastructure is D+. Therefore, disaster mitigation and infrastructure management has been one of

the main priorities of today's structural engineering community.

Structural health monitoring (SHM) [1] is considered as a process of monitoring the performance of a structure to decide whether or not the structure continues to perform its desired function. The traditional way to monitor civil structures is a visual inspection where inspectors visually assess the structural members by looking for any sign of distress. In recent years, vibration sensors have been utilized to evaluate local and global health conditions of structures by performing necessary data analysis to extract dynamical properties of the structures. Dynamical characteristics of civil infrastructures are exposed to deteriorate and change over time due to severe earthquake, strong winds or other traffic loads. Once the structural parameters are identified from the measured vibration data, decisions and recommendations can be appropriately made about repairs and maintenance actions.

Vibration data obtained from civil structures allows damage detection, identification of damage location, and may even classifies the damage and predicts future distress. The process of assessment starts with detecting existing damage, and then determining the location and severity of damage; thus it is possible to estimate the remaining life of the structure. As knowledge of SHM to evaluate local and global health conditions of structures is insufficiently diffused, infrastructure owners have started exploring modern sensing techniques (i.e., wireless sensors, mobile sensors and non-contact devices) that can facilitate long-term monitoring of large-scale structures.

1.2 Modern Sensing and Big Data

Wireless sensor network (WSN) has recently gained significant attentions in the field of SHM where various civil structures could be dynamically assessed in ease. This technology has proven its efficiency in monitoring acceleration and displacement of large-scale structural systems like bridges, building and dams. Compared to wired sensors, wireless sensors are inexpensive and easier to install with less labour-intensive process, thereby leading to significant cost-saving to the infrastructure owners [5]. The hardware design of wireless sensors is as important as the embedded software design that operates each wireless sensor within a network. Most existed prototype wireless sensors recently are passive devices, which only measure the response of structures. In future, wireless sensors with actuation and signal processing capabilities are expected to be more powerful to monitor large-scale structures.

In [7], a comparison is studied between two popular wireless sensors, namely Imote2 and Narada, which are utilized for SHM of existing buildings and other infrastructure. They are tested, evaluated, and compared in three different categories; sensor options, data collection and antenna signal strength. These two wireless sensors, shown in Fig. 1.1, can be attached to a structure to assess its performance by monitoring displacement, accelerations, temperature, and other loads and responses in a continuous basis. Imote2 is convenient to use due to its stacking system, as the stocked boards make it easy to be attached to structures with a little space. On the other hand, Narada provides a distinct benefit of its ability in using any external sensors with the system [7] which makes it more versatile. Consequently, the use of both wireless sensors show a great performance and encouragement to be exploited in SHM.

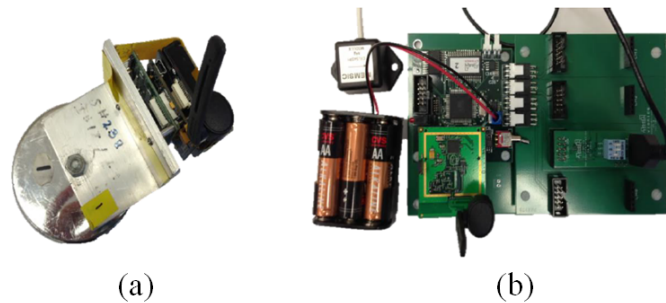


Figure 1.1: Wireless sensing unit of (a) Imote2 and (b) Narada [7]

With increasing trend of long-term monitoring of large-scale structures, the processing, transmission and analysis of big data has been a major constraint. In fact, WSN has shown a serious challenge in data transmission when collecting a large amount of data using multiple sensors. The use of multiple sensing transducers with higher sampling frequency produces a large volume of data from each channel which consequently lead to a major transmission issue in a network [2, 3, 4]. Moreover, WSN is also associated with packet loss and missing data due to the limited bandwidth of wireless sensors. A large amount of data measured from multiple WSNs requires accurate time synchronization to be synced with same time stamps. Even using wired sensors, transmission and storage of large data in long-term SHM stipulates massive computational and data mining capabilities.

A common solution to large data transmission issue is to implement compression algorithms where the rate of data compression should be sufficiently adequate to allow accurate data characterization [8]. In the context of SHM applications, data compression seems to be extremely useful since it can diminish a large volume of data without losing significant characteristics that are very sensitive to perform SHM. The process of data collection using wireless sensors is illustrated in Fig. 1.2. In general, network jam occurs while transmitting the data from the sensing units to the base

station due to the limited bandwidth of the WSN, thus the observed data renders to be not useful unless a robust data compression technique is applied to convert the large amount of data into fewer measurements. Reconstruction process can be then applied to the compressed signal to represent the desired size of data.

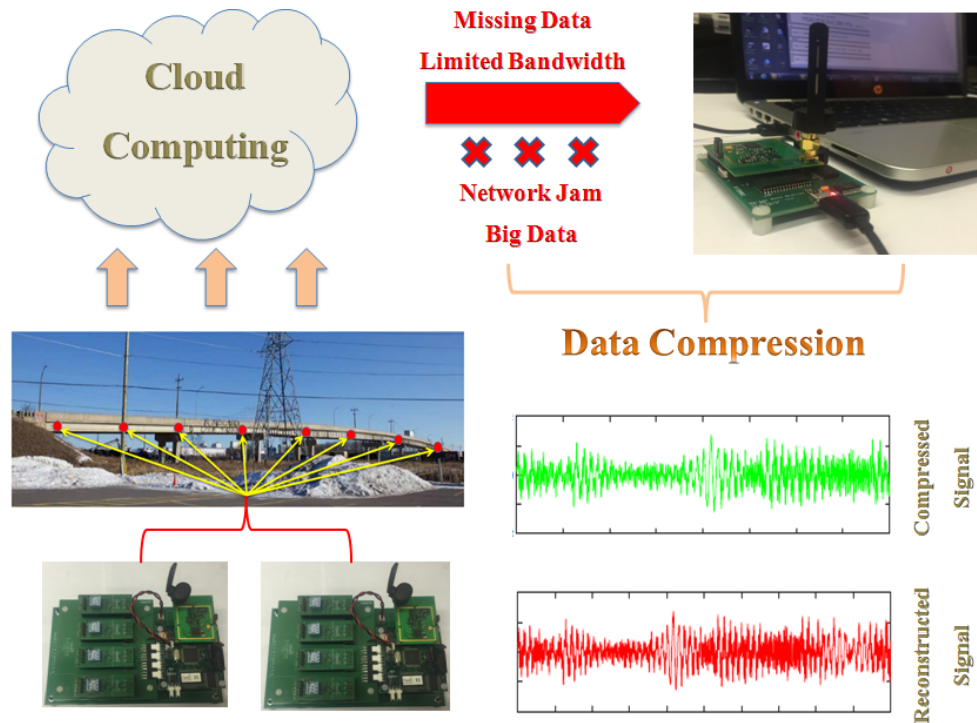


Figure 1.2: Formation of big data in modern sensing network and their potential challenges

1.3 Data Compression Techniques

Data compression is known as storing data in a way which requires fewer measurements to represent it than its typical form. Data compression uses several compressing techniques and software solutions to reduce the size of data. It plays a significant role in terms of solving the issue of transmission quality that causes packet loss or missing data. Compressing techniques can handle big data by storing the original information into fewer measurements and then transmit to the receiver. When the transmission

of compressed information is successfully completed, it is possible to recover the data using data reconstruction techniques.

Recent literature includes many works that address the performance of data compression to real structure data. For instance, a study [9] explores principal component analysis-based data compression through an experimental study by the electro-mechanical impedance-based wireless sensing. Principal component analysis is used to diminish dimensionality and eliminate undesired elements of the raw data obtained from the macro-fiber composite patch. A big data technique, known as MapReduce, has been investigated [10] to handle the large volume of data in order to perform damage diagnosis. The MapReduce technique is implemented with a spark platform to parallelize the big data efficiently. Compressive sensing (CS) has recently become a promising technique that can be applied using various methods such as l_1 -norm minimization (LNM). Since most signals of structural systems naturally have a sparse representation in a basis, CS via LNM exploits the advantage that one can recover sparse signals from fewer samples [11].

1.4 Literature Review of Data Compression Methods

A recent study [20] focuses on reducing data transmission payloads in WSN for operational modal analysis of civil structures using two different spectral estimation approaches which support non-uniform-in-time data sampling at the sub-Nyquist rate. These two approaches can effectively satisfy transmission bandwidth constraints in WSN. The first approach takes the advantage of Compressed Sensing (CS) theory to address sub-Nyquist randomly sampled data while the acceleration signals are sparsely represented in the frequency domain. The second approach relies on a power spectrum blind sampling technique, assuming deterministic sub-Nyquist sampling and

dealing with the acceleration signals as wide-sense stationary stochastic processes regardless of sparsity conditions.

The theory of CS relies on two principles that play a significant role to make this workable which the signal must be sparse and incoherent. A sparse representation is a signal in which most of the elements are zero, whereas incoherence extends the relation between time and frequency to express the idea of having a sparse representation in the basis, where a compressible signal can be captured effectively through a number of incoherent measurements. In fact, the large volume of collected data and the number of sensors attached to the structure can be considerably reduced by the application of CS [15]. It is possible to lower the sampling frequency and diminish the number of sensors by applying implicit data reconstruction as desired through CS.

Several researchers have introduced the theory and application of CS which facilitates data compression and enhances data reconstruction. There are three different types of recovery algorithms presented in [11], known as convex optimization algorithms, greedy algorithms and combinatorial algorithms. Moreover, other applications of CS, namely data separation and recovery of missing data, are exploited to apply this theory. The potential is to increase the efficiency of data transmission by applying CS as one technique of data compression, and then achieving accurate reconstruction of compressed signals. CS theory proves that certain signals and images with sparse and incoherent representation can be recovered from fewer samples or measurements.

The challenges of transmitting and monitoring a large amount of data in using wireless sensors has been addressed [12] through l_1 -magic tool, and then the results are compared with wavelet and Fourier orthogonal bases and Huffman coding. CS can exploit the sparsity of mode shapes and recover data from undersampled signals to

avoid failure in data collection. In addition, several CS recovery schemes, such as least square with l_1 -norm regularization, can be interpreted using Bayesian compressive sensing (BCS) [16]. The BCS reconstruction algorithm utilizes the sparse Bayesian learning method to deduce probability distribution over the basis coefficient in order to cease the basis term that is not contributed considerably to the reconstructed signals. Synthetic spike signals with various sparsity levels have been considered to apply the BCS proposed algorithms using two real structural systems.

Application of CS through LNM has been performed using two different cases [18]. Vibration signals obtained from a cantilever beam and a building model are compressed with a certain ratio and then reconstructed using LNM, where results prove that this method can facilitate data compression and enhance data recovery. Furthermore, the application of CS through group sparse optimization has been investigated using data collected from a bridge by WSN [17]. As measured vibration signals obtained from several sensors attached to a structure generate same sparse structure in frequency domain, data can be reconstructed from incomplete measurements by exploiting the development of the group sparse optimization algorithm.

A study [14] has presented the performance of two damage detection and localization techniques, known as automatic relevance determination and Wiener filter. Automatic relevance determination uses estimated time-series models from structural responses whereas Wiener filter utilizes the CS-reconstructed signals. Both methods have proven effectiveness of CS application in terms of maintaining the significant characteristics of a signal to represent the original data. Moreover, as testing of civil structures normally generates a large amount of data, energy consumption can affect the lifetime of wireless sensors which may become a serious issue when using WSN. However, the theory of CS includes: the sparse representation of the signal,

the measurement matrix that should satisfy Restricted Isometry Property, and the reconstruction algorithms [19]. This approach can measure the general robustness of CS. The application of this theory has ensured accuracy of data reconstruction and balancing the network energy consumption.

Modeling and harnessing sparse and low-rank data structure has presented [22] a new paradigm for SHM in terms of dynamics, identification and damage detection. It is discussed how beneficial is to define sparsity in order to develop system identification and damage detection. Harnessing sparse and low-rank data structure can be effectively modelled and processed by using mathematical approaches such as sparse representation and CS, low-rank decomposition and completion. A research [13] focuses on the application of modal analysis that may be expressed as an atomic norm minimization problem to effectively achieve a perfect recovery for mode shapes and natural frequencies. This method considers five measurement schemes which are: uniform sampling, synchronous random sampling, asynchronous random sampling, random temporal compression and random spatial compression. Digital cameras are cost-effective vision sensors that can continuously monitor and record vibrations of civil structures by providing data in two dimensions. A study of CS technique [21] explores efficiency of data transmission and recovery of the large scale image data in order to diagnosis a structures performance. Results show that it can recover images accurately, without losing diagnostic quality of structural health, from highly under-sampled measurements.

CS provides a data loss recovery that can be embedded into smart wireless sensors and increases communication reliability without retransmitting the data, where another proposed approach aims to save power by reducing communication [28]. The key idea of CS-based approach is that a transformed signal is transmitted where it

is produced by projecting the row signal onto a random matrix, instead of transmitting the signal acquired by the sensor. The random matrix is made to meet the requirements of data recovery where the row signal can be effectively reconstructed from the received incomplete transformed signal as it is compressible. In addition, a new data coding and transmission method is proposed [29] to enhance reliability of WSN utilized in SHM. This proposed method is comprised of two stages: a source coding stage to compress redundancy and a redundant coding stage to inject artificial redundancy to enhance transmission reliability. In both studies [28, 29], techniques are implemented into Imote2 smart sensor platform where the embedded programs are tested through communication experiments.

Discrete Cosine Transform (DCT) is an orthogonal transform method that has been widely applied in image/video processing research. Several researchers [30, 31, 32, 33] have studied this method in terms of its efficiency in image/video compression. Recently, a new method of image compression has been proposed [32] using DCT which is superior to improve the performance of conventional vector quantization algorithm and hybrid DCT-vector quantization technique. Vector quantization is a lossy image compression technique that has a simple decoding structure and can provide a high compression ratio in image coding systems. The main idea of multistage vector quantization is that the whole vector quantization process is carried out in several successive stages where it can reduce the codebook size and computing time and render small quantization distortion. Moreover, steerable DCT has been proposed [33] to rotate pairs of basis vectors in a flexible way, and enables precise matching of directionality in each image block to achieve improved coding efficiency. The optimal rotation angles for steerable DCT can be regarded as a solution of a suitable rate-distortion problem.

The image/video transmission system has been analyzed to perform compression by discarding the redundancy in image data. DCT [34] can present source encoder and decoder; source encoder of the original image starts with transformation via a quantizer and entropy encoder, and then pass it through the transmission channel while the source decoder performs the inverse of the same process in order to generate the reconstructed image. As a result, correlations can be used to predict the pixels from their neighbouring pixels, and transformation can exploit the fact that the bits of an individual pixel is considered small compared to large visual contributions of a pixel that can be estimated when looking at its neighbouring pixels. It is proved that DCT can decorrelate the image data and efficiently perform compression. However, there is currently no research that explores DCT in data compression, specially the bid data associated with SHM.

1.5 Gap Areas

There has been a significant growth in modern sensing technology to capture good quality data. However, with increasing demand for long-term monitoring of large-scale structures, the resulting big data poses significant challenges to the signal processing and accurate interpretation of the data.

- With increasing sampling frequency and the number of sensing transducers in a WSN, the large amount of data collected from any structural system often causes missing data, network jam or packet loss while transmitting the data, resulting in poor quality of data.
- Piezoelectric wired sensors are equipped with excellent sensitivity and capable of utilizing higher sampling frequencies for long-term SHM. However, while transferring such big data to the central processor, it demands massive data storage and processing capability.
- Data compression techniques could be valuable to achieve a desired compression rate. However, accuracy of data reconstruction is very important where quality of reconstructed data changes when using different rates of data compression. Several studies have presented the application of various compression techniques while there is a lack of studies that focus on accurate damage detection using undersampled data.
- Most of the research of compressed sensing is focussed on image or video-based data. There has been a limited research on time-histories of vibration data. The LNM is validated using different simulation models, however its performance needs to be checked through adequate experimental models and real-life data.

On the other hand, DCT technique has proven excellent capability in image compression, however, it is not explored for data compression yet.

- The existing data compression techniques are validated by comparing the time structure of original and reconstructed data. However, there is a limited research of evaluating the performance of data compression techniques in identifying modal parameters of the structures.
- Apart from simulation models, different experimental models with a wide range of dynamical characteristics are needed to be explored to validate any newly developed data compression techniques.

1.6 Thesis Objectives

The main objective of this thesis is to develop a robust and faster data compression technique to analyze big data in SHM. The key objectives are listed corresponding to the gap areas mentioned above.

- Explore DCT as a potential data compression tool for vibration data.
- Compare the performance of DCT with LNM with a wide range of simulation and experimental models.
- Ensure an accurate data reconstruction is achieved under a broad range of compression rates. Since compression ratios play a significant role in terms of evaluating the performance of data compression techniques, various rates need to be investigated to check effectiveness and accuracy.

- Apart from comparing merely time-structure of data, develop a newer system identification algorithm to evaluate the performance of data compression techniques in identifying modal parameters.
- The proposed data compression and recovery needs to be checked under different real-life conditions including discrete damage, closely spaced modes, low energy modes and measurement noise using a wide range of experimental models.

The thesis is outlined as follows. First, a background of various data compression techniques and the proposed algorithm is presented in **Chapter 2**. In **Chapter 3**, the adopted sensing devices are validated using several experimental studies. The proposed algorithms are then validated using a suite of numerical studies in **Chapter 4** followed by several experimental and full-scale studies in **Chapter 5**. Finally, the key conclusions of the proposed research are discussed in **Chapter 6** followed by the major research contributions and future work.

Chapter 2

Proposed Method

In this chapter, two different data compression techniques are explored to perform data compression. Both methods are proposed to be considered as important tools that can be exploited in data compression for SHM applications. The first method, namely l_1 -norm minimization (LNM) technique, is based on classical theory of compressed sensing (CS) while Discrete Cosine Transform (DCT) has gained significant attention in the field of image compression. The essential criteria and principles of both methods are presented to explain the proposed methodology. A newer system identification (i.e., Time-frequency Blind Source Separation (TFBSS)) is explored next followed by the formulation of proposed data compression technique using classical equation of motion of a dynamical system. Apart from time structure of the original data, the accuracy of proposed data compression technique is then validated using identified modal parameters of the structures.

2.1 L_1 -norm Minimization

l_1 -norm minimization (LNM) [26, 27] refers to determine minimum solution of l_1 -norm of an undetermined linear system $b = Ax$ that is comprised of more number of unknowns than the number of available equations. With the aid of compressed sensing (CS), this norm achieved sparse solutions to a system of linear equations. Two important principles are required to achieve the minimum l_1 -norm solution: (a)

the signal x must be sufficiently sparse and (b) the sensing matrix A is incoherent with basis under which x can be exactly recovered by calculating the solution of l_1 -norm given by following optimization problem [25]:

$$\min_x \|x\|_1 \quad \text{subject to } b = Ax \quad (2.1)$$

Using CS theory, it takes the advantage of the fact that most signals have a sparse representation. For example, biomedical signals (i.e., ECG/EMG signals) are sparse in time domain whereas the vibration signals are sparse in frequency domain. Using the $N \times N$ basis matrix ψ , with ψ_i vectors as columns and the modal response q , the signal x can be expressed as:

$$\begin{aligned} x &= \sum_{i=1}^N \psi_i q_i \\ x &= \Psi q \end{aligned} \quad (2.2)$$

where q is the $N \times 1$ column vector of selected measurement $q_i = \langle x, \psi_i \rangle = \psi_i^T x$ and T indicates the transpose. Consider the problem of reconstructing as a vector $x \in R^N$ from linear measurements $y \in R^p$ of x in the undersampled expression in Eq. 2.2.

$$y_p = \langle x, \phi_p \rangle \quad (2.3)$$

$$y = \Phi x = \Phi \Psi q = \Theta q$$

where $p = 1, \dots, m$ in the number of compressed samples and $m \ll N$. Φ is the $m \times N$ measurement matrix [18]. Since this signal x is sparse, reconstruction is possible by solving convex optimization $\hat{q} = \|\tilde{q}\|_{l_1} = \sum_{i=1}^N |\tilde{q}_i|$ where the objective is to find best estimated q that yields to LNM [18]:

$$\hat{q} = \|\tilde{q}\|_{l_1} \quad \text{with an equality constraint of } \Theta \tilde{q} = y \quad (2.4)$$

Therefore, the reconstructed signal can be expressed as:

$$x_r = \Psi \hat{q} \quad (2.5)$$

Primary-dual linear programming algorithm is used in this study with its associated l_1 -magic tool. This method takes advantage of the idea that many structural responses naturally have sparse representation in a basis in the frequency domain.

2.2 Discrete Cosine Transform

The Discrete Cosine Transform (DCT) separates an image or data into specific parts with respect to the significant features of the signal and transforms a signal or image from spatial domain to the frequency domain. The DCT gives a sparse set of basis vectors where the principle DCT coefficients that contain fewer measurements are stored to represent the entire data instead. Each DCT considers N real basis vectors where components are cosine functions. It de-correlates an image data and each transformed coefficient is encoded independently without losing compression efficiencies.

DCT is a linear orthogonal transformation of a signal and it is equivalent to discrete Fourier transform (DFT) in case of a real and even function. Compared with DFT, DCT can be performed only using real number. Therefore, DCT is superior to DFT in computational complexity. After performing DCT, the block can be divided into 2 sub-bands: low frequency sub-band which contains most of the important visual parts of the image, and high frequency sub-band which contains details and textures of the image. Generally speaking, low frequency coefficients are more important than high frequency coefficients because the values of high frequency coefficients are usually closed to zero. Of all the DCT coefficients, $X(0,0)$ is called DC coefficient and other coefficients are called AC coefficients. Due to non-importance of high frequency sub-band, the high frequency sub-band is usually removed for compression purpose. DCT has several advantages over signal processing tools [34]: (1) it has the ability to pack

energy in the lower frequencies for image data. (2) it can reduce the blocking artefact effect and this effect results from the boundaries between sub-images as they become visible. The DCT provides a very good compromise between information packing ability and computational complexity.

In general, DCT depends on the assumption that pixels in images possess a certain level of correlation with their surrounded pixels, where DCT is considered an orthogonal transformation that has been widely used in image/video compression. Consequently, the value of pixels is predicted from their respective neighbouring pixels while exploiting the level of correlation in a given image. In this way, the transformation is used to plot correlated spatial data into uncorrelated transformed coefficients. Few key properties of DCT are presented next [30]:

(a) Decorrelation

Decorrelation of the input signal transforms its representation in which the set of data values is sparse, thereby leading to compact the information content of the signal into fewer number of coefficients [35]. The advantage of DCT in image transformation is the possibility of removing redundancy between neighbouring pixels which leads to achieve uncorrelated transform coefficients that independently interacts with encoding.

(b) Compaction of Energy

Energy compaction is the ability to pack the energy of the spatial sequence into as few frequency coefficients as possible which is important for image compression as only transmission of few coefficients instead of the whole set of pixels is required if compaction is high. Efficiency of compression scheme can be measured by its

capability to store input signals into as few measurements as possible which qualifies the quantizer to discard insignificant coefficients with relatively low amplitude. This proves that DCT exhibits energy compaction for highly correlated images.

(c) Separability

The advantage of separation can be highly exploited in compression. The reconstructed outputs can be computed in two separate steps by operations on rows and columns of images. Therefore, these steps are identically considered for the inverse DCT determination.

(d) Symmetricity

DCT is characterized by a symmetric matrix, known as the symmetric cosine transform, which makes its covariance matrix more tractable for the symmetric cosine transform. It reveals that the transformation matrix of rows and columns can be predetermined offline, and then applied to the image; thus orders of magnitude improvement can be presented to assess efficiency.

(e) Orthogonality

As DCT basis functions are orthogonal, the inverse transformation matrix of A is equal to its transpose i.e. $A^{-1} = A^T$; where T donates transpose. Therefore, this advantage can be exploited in reduction and application of the inverse DCT computation.

The aim is to decorrelate the pixels of the input image in order to compact the neighbouring pixels into fewer coefficients while the quantizer reduces the number of the transformed measurements. Thus it is possible to reduce accuracy of those bits.

Entropy encoding discards redundancy by removing bit patterns repeated from the output of the quantizer in order to achieve compression [30], as steps are illustrated in Fig. 2.1.

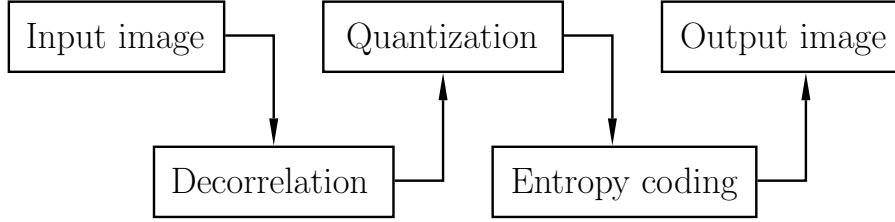


Figure 2.1: Flowchart of the DCT [30]

The performance of DCT in image compression can be estimated by applying criteria of compression ratio (CR) and the quality of measurements of the reconstructed image (PR) [30]. CR is the ratio between the size of the original and compressed image as:

$$CR = \frac{n_1}{n_2} \quad (2.6)$$

Mean Square Error (MSE) measures the rate of distortion in the reconstructed image through [30]:

$$MSE = \frac{1}{HW} \sum_{i=1}^H \sum_{j=1}^W [X(i, j) - Y(i, j)]^2 \quad (2.7)$$

In brief, DCT has been widely exploited by modern standards of video coding. This method of transformation aims to decorrelate the image data while each transform coefficient after decorrelation can be independently used for processing without losing compression efficiency.

In order to illustrate the DCT method and its data compression, a discrete signal x is used to generate the DCT coefficients X as illustrated in Fig. 2.2(a) where Fig. 2.2(b) is its DCT coefficients. This is equivalent to the pre-multiplication of x by the

matrix ϕ as:

$$[\mathbf{X}] = [\phi][x] \quad (2.8)$$

where the input signal x is an $N \times 1$ vector and X is the $N \times 1$ DCT vector. The DCT computation is defined as:

$$\mathbf{X}[\mathbf{k}] = \sqrt{\frac{2}{N}} C_k \sum_{n=0}^{N-1} \mathbf{x}[n] \cos \left[\frac{(2n+1)k\pi}{2N} \right] \quad (2.9)$$

where the coefficient C_k is given as:

$$C_k = \begin{cases} \frac{1}{\sqrt{2}} & \text{if } k = 0 \\ 1 & \text{if } k > 0 \end{cases} \quad (2.10)$$

with $0 \leq (n, k) \leq N - 1$.

The process of image compression using DCT may be described as follows:

- First, the image is broken into blocks of pixels.
- The DCT is applied to each block, working from left to right and top to bottom.
- Each block is compressed using the quantization table.
- The array of compressed blocks that comprise the image is stored in a drastically reduced amount of space.

The reconstruction of image is performed through decompression which is a process that uses the Inverse Discrete Cosine Transform (IDCT). The DCT coefficient vector X is sparse with the energy of the signal (norm) concentrated on few components (k values). Therefore, one can neglect small components in order to obtain reduction in the data norm. This can be achieved by the threshold function which equates any DCT coefficient below a certain threshold level to zero. The compressed

signal can be then reconstructed in the receiver using the IDCT, which is expressed as [34]:

$$\mathbf{x}[\mathbf{n}] = \sqrt{\frac{2}{N}} \sum_{k=0}^{N-1} C_k \mathbf{X}[k] \cos \left[\frac{(2n+1)k\pi}{2N} \right] \quad (2.11)$$

As illustrated in Fig. 2.2, an example shows the application of the proposed DCT method in data compression using a sine wave signal, where (a) indicates the original and reconstructed signal respectively, and (b) presents the DCT coefficients stored into fewer measurements. The threshold level is then appropriately set to discard samples outside the range that represents redundancy. This example shows how DCT data compression can maintain the significant features of a signal.

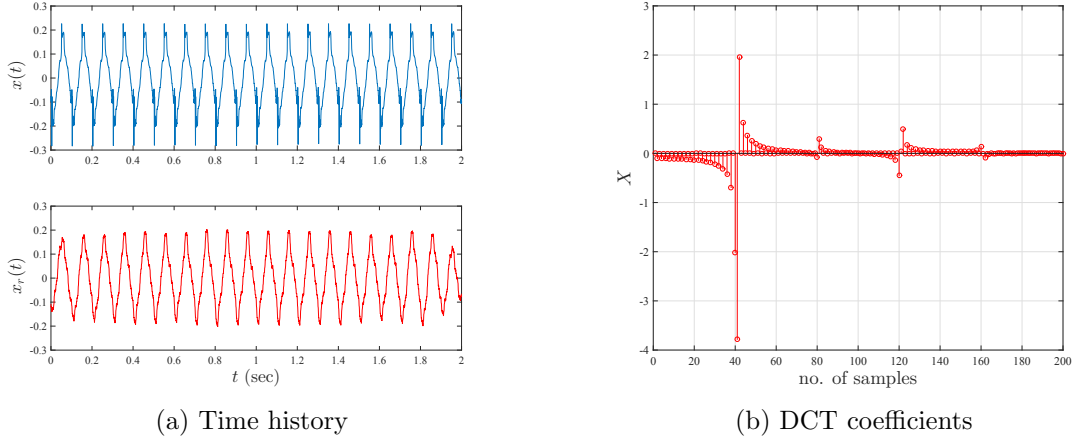


Figure 2.2: The performance of DCT method in data compression

The flowchart shown in Fig. 2.3 illustrates the process of applying the proposed method to achieve data compression. It stores all samples into as few DCT variables as possible, where DCT coefficients of vibration signals decreases the data norm. The threshold level of any rate means that all measurements with a magnitude placed below the threshold limit would be considered zero, thus they are not included in the processing. A lower percentage of threshold results in lower compression. The compressed signal can be then recovered by using IDCT through Eq. 2.11, where the

threshold level is appropriately set to discard redundancy before applying IDCT to reconstruct the signal.

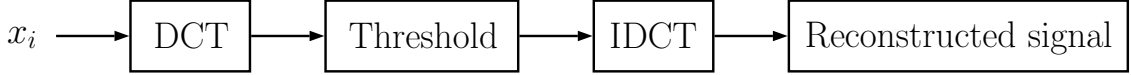


Figure 2.3: Flowchart of the implementation of DCT

2.3 Time-Frequency Blind Source Separation

Blind source separation (BSS) [36] is recently explored as a potential signal decomposition tool for structural system identification. In this thesis, another form of BSS is explored using time-frequency (TFBSS) distribution of spatial Wigner-Ville spectrum (SWVS). The stochastic signals are explicitly assumed as:

$$\mathbf{x}(t) = \mathbf{A}\mathbf{q}(t) + \mathbf{d}(t) \quad (2.12)$$

where $\mathbf{x}(t) = [x_1(t), \dots, x_m(t)]^T$ is the vector of measurement, $\mathbf{q}(t) = [q_1(t), \dots, q_n(t)]^T$ is vector of sources. \mathbf{A} is the $m \times n$ unknown full-rank mixing matrix as $m \geq n$. $\mathbf{d}(t)$ is an independently and identically distributed noise vector, independent of the sources as:

$$E \left\{ \mathbf{d} \left(t + \frac{\tau}{2} \right) \mathbf{d}^H \left(t - \frac{\tau}{2} \right) \right\} = \delta(\tau) \sigma^2 \mathbf{D}_m. \quad (2.13)$$

\mathbf{D}_m denotes the identity matrix of size m , $\delta(\tau)$ the Dirac δ function, \cdot^H is conjugate transpose, and σ^2 denotes the unknown variance of the noise. At time t and lag τ , the covariance of $\mathbf{q}(t)$ is expressed:

$$\mathbf{R}_{\mathbf{q}}(t, \tau) = E \left\{ \mathbf{q} \left(t + \frac{\tau}{2} \right) \mathbf{q}^H \left(t - \frac{\tau}{2} \right) \right\} = \text{diag} [\rho_1(t, \tau), \dots, \rho_n(t, \tau)]. \quad (2.14)$$

Using the source un-correlation assumption, $\rho_i(t, \tau) = E \left\{ q_i \left(t + \frac{\tau}{2} \right) q_i^* \left(t - \frac{\tau}{2} \right) \right\}$, $i = 1, \dots, n$, where \cdot^* donates complex conjugate. Using the covariance matrix $\mathbf{R}_{\mathbf{x}}(t, \tau)$ of

$x(t)$ is:

$$\mathbf{R}_{\mathbf{x}}(t, \tau) = \mathbf{A} \text{diag}[\rho_1(t, \tau), \dots, \rho_n(t, \tau)] \mathbf{A}^H + \delta(\tau) \sigma^2 \mathbf{D}_m. \quad (2.15)$$

$\mathbf{R}_{\mathbf{x}}(t, \tau)$ defines a time-lag representation of the nonstationary signal vector $\mathbf{x}(t)$. A strictly equivalent TF representation of $\mathbf{x}(t)$ is obtained via the Fourier transform of $\mathbf{R}_{\mathbf{x}}(t, \tau)$ with respect to τ , yielding the spatial Wigner-Ville spectrum \mathbf{S} of $\mathbf{x}(t)$,

$$\mathbf{S}_{\mathbf{x}}(t, f) = \int_{-\infty}^{+\infty} \mathbf{R}_{\mathbf{x}}(t, \tau) e^{-j2\pi f\tau} d\tau \quad (2.16)$$

For a given TF location (t, f) , $\mathbf{S}_{\mathbf{x}}(t, f)$ is a square matrix of size m whose diagonal entries contain the auto Wigner-Ville spectra of the observations and nondiagonal entries contain cross-Wigner-Ville spectra. In the TF plane, it becomes [37]:

$$\mathbf{S}_{\mathbf{x}}(t, f) = \mathbf{A} \mathbf{S}_q(t, f) \mathbf{A}^H + \sigma^2 \mathbf{D}_m \quad (2.17)$$

where $\mathbf{S}_q(t, f)$ is a diagonal matrix for any (t, f) , since it is Fourier transform of the diagonal matrix $\mathbf{R}_q(t, \tau)$.

Let \mathbf{W} be an $n \times m$ full-rank matrix such that $\mathbf{W}(\mathbf{A}\mathbf{A}^H)\mathbf{W}^H = \mathbf{I}_n$, where \mathbf{W} represents whitening matrix. Define another matrix $\mathbf{U} = \mathbf{W}\mathbf{A}$, where \mathbf{U} is a unitary matrix satisfying,

$$\mathbf{A} = \mathbf{W}\mathbf{U}. \quad (2.18)$$

\mathbf{U} can be derived from the eigen vectors of the following matrix:

$$\mathbf{S}_{\mathbf{x}}(t, f) = \mathbf{U}\mathbf{S}_q(t, f)\mathbf{U}^H \quad (2.19)$$

Since $\mathbf{S}_q(t, f)$ is diagonal for any (t, f) , and since \mathbf{U} is unitary, \mathbf{U} diagonalizes $\mathbf{S}_{\mathbf{x}}(t, f)$ for any (t, f) . Once \mathbf{U} is estimated, \mathbf{A} can be found using Eq. 2.18 and the sources \mathbf{q} are estimated using Eq. 2.12.

In order to illustrate the performance of TFBSS, a simple example involving a mixture of sine signals is considered using Eq. 2.20 where $\omega_1 = 1.5$, $\omega_2 = 2.8$ and

$\omega_3 = 4$ Hz. The sine signals are generated using Eq. 2.20 and their corresponding Fourier spectra are shown in Fig. 2.4. TFBSS is then applied to those signals and the Fourier spectra of separated modal responses are shown in Fig. 2.5. The results reveal that TFBSS is capable of separating modal responses very accurately.

$$A = \begin{bmatrix} 7 & -3 & 5 \\ -4 & 7 & -5 \\ 3 & -5 & 7 \end{bmatrix} \begin{bmatrix} \sin(\omega_1 t) \\ \sin(\omega_2 t) \\ \sin(\omega_3 t) \end{bmatrix} \quad (2.20)$$

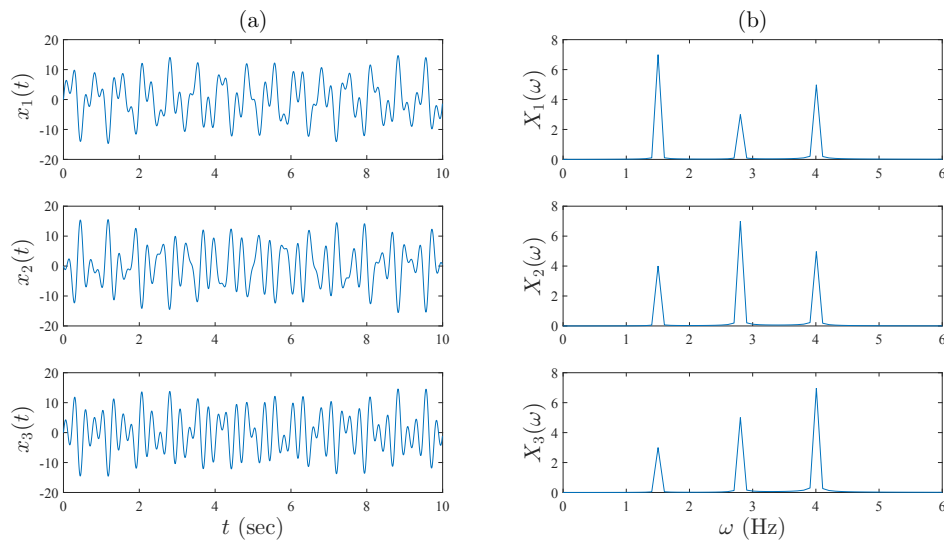


Figure 2.4: (a) Time history and (b) Fourier spectra of the mixture of sine signals

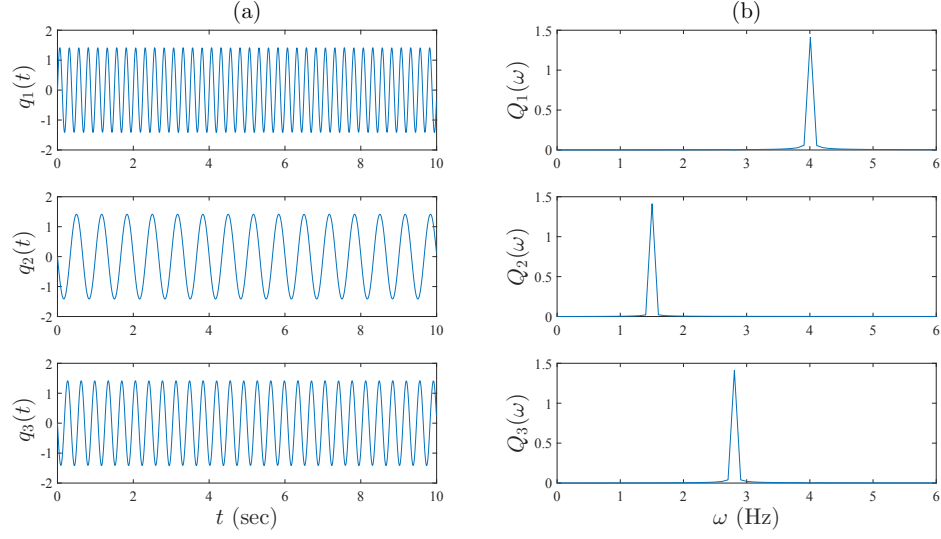


Figure 2.5: (a) Time history and (b) Fourier spectra of modal responses obtained from the TFBSS

2.4 Proposed Methodology

Consider a linear, classically damped and lumped-mass n degrees-of-freedom (DOF) structural system, subjected to a wide-band random input force, $\mathbf{u}(t)$:

$$\mathbf{M}\ddot{\mathbf{x}}(t) + \mathbf{C}\dot{\mathbf{x}}(t) + \mathbf{K}\mathbf{x}(t) = \mathbf{u}(t) \quad (2.21)$$

where, $x(t)$ is a vector of displacement response at DOFs. \mathbf{M} , \mathbf{C} and \mathbf{K} are mass, damping and stiffness matrix, respectively. The solution to Eq. 2.21 for any dynamical system can be formulated using the state-space model with following form:

$$\bar{\mathbf{x}} = \begin{bmatrix} x_1 \\ x_2 \end{bmatrix} \quad (2.22)$$

$$\dot{\bar{\mathbf{x}}} = \mathbf{A}\bar{\mathbf{x}} + \mathbf{B}\mathbf{u} \quad (2.23)$$

$$\mathbf{y} = \mathbf{C}\bar{\mathbf{x}} + \mathbf{D}\mathbf{u} \quad (2.24)$$

where \mathbf{A} is the state matrix, \mathbf{B} is input matrix, \mathbf{C} is the output matrix, and \mathbf{D} is transmission matrix. Under broad-band excitation $\mathbf{u}(t)$, the resulting solution of Eq. 2.21 can be written in terms of an expansion of vibration modes:

$$\mathbf{x} = \Phi \mathbf{q} \quad (2.25)$$

where, \mathbf{x} and \mathbf{q} is the DCT-assisted reconstructed response and modal coordinate matrix, respectively. $\Phi_{m \times n}$ is the modal transformation matrix. n and m are the number of modal responses and measurements, respectively. Comparing Eq. 2.25 with Eq. 2.12, we get following from Eq. 2.19:

$$\mathbf{S}_x(t, f) = \mathbf{V} \mathbf{S}_q(t, f) \mathbf{V}^H \quad (2.26)$$

Once \mathbf{V} is estimated using Eq. 2.26, Φ can be estimated using:

$$\Phi = \mathbf{W} \mathbf{V}. \quad (2.27)$$

Once Φ is obtained, \mathbf{q} can be found using Eq. 2.25:

$$\mathbf{q} = \Phi^{-1} \mathbf{x} \quad (2.28)$$

Once the modal responses are obtained, the modal frequencies and damping can be successively found. Finally, the flowchart of the proposed method is shown in Fig. 2.6.

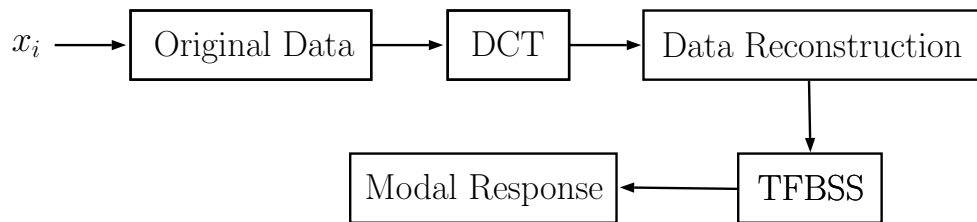


Figure 2.6: Flowchart of the proposed method

Chapter 3

Validation of Wireless Sensor Network

In this chapter, the performance of wireless sensor utilized in this thesis is validated with various other sensor devices to validate their capabilities of monitoring vibration of low frequency systems. A wireless sensor, namely Narada, is used in this research. The performance of Narada units are validated through a suite of experimental studies before employing different data compression techniques with the sensor boards.

3.1 Background

A brief background of Narada sensor is illustrated in the following section.

3.1.1 Narada

The Narada wireless sensing unit is developed by CivionicsTM [6]. It can be attached to a structure to measure its acceleration. Narada consists of sensing units, sensing transducers and a base station as shown in Fig. 3.1. A maximum of four channels can be used per sensing unit, while the base station can wirelessly communicate with multiple sensing units at the same time. The maximum allowable sampling frequency is 10,000 Hz whereas the antenna range is considered as 50 m [7]. However, with increasing number of sensor units, the achievable sampling frequency reduces significantly along with missing data and packet loss. In order to explore WSN, four Narada sensors were utilized to conduct these studies.

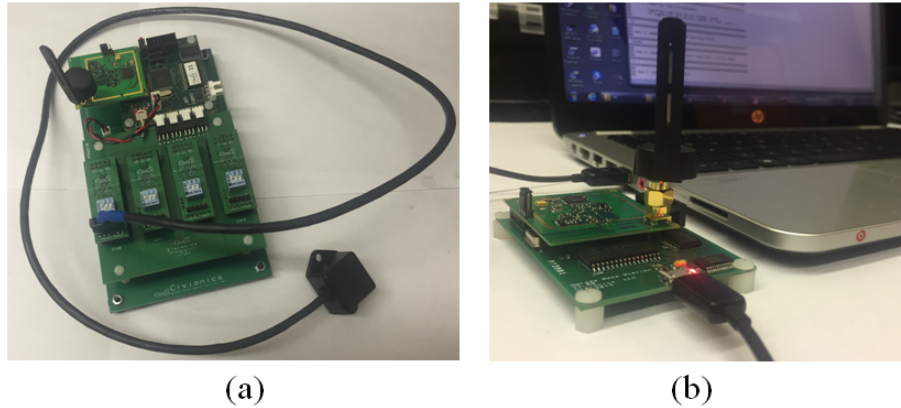


Figure 3.1: Narada WSN: (a) one sensing transducer attached to a Narada unit, (b) base station attached to a laptop

3.1.2 Other Sensing Devices

The Trigno wireless system is capable of monitoring accelerations and displacement of different dynamic systems, especially with higher frequencies. This wireless sensor as illustrated in Fig. 3.2(a) is equipped with great features for use such as: transmission range of **20 m**, **signal sampling rate up to 2000 Hz**, integrated triaxial accelerometer, self-contained rechargeable battery lasting a minimum of 7 hours, battery charge monitoring and status indicator, auto shutoff [23]. Its base station communicates with a computer through a USB link after installing EMGworks software. The Trigno wireless system has proven its reliability and efficiency to be used for data collection in SHM even though it is designed for other purposes.

Apart from Trigno, a digital camera is also used for validation purpose. Digital cameras are cost-effective vision sensors that can continuously monitor and record vibrations of civil structures by providing data of two dimensions. This high speed camera, shown in Fig. 3.2(b), is equipped with distinct features that can be exploited in monitoring the performance of civil structures. As the resolution of high speed cameras control the rate of sampling frequency, the sampling frequency is selected as

60 Hz. In order to test the functionality of Narada devices, both Trigno and a high speed camera were borrowed from Kinesiology laboratory of Lakehead University with the assistance of Dr. Carlos Zerpa, and the performance of Narada is assessed for SHM applications.

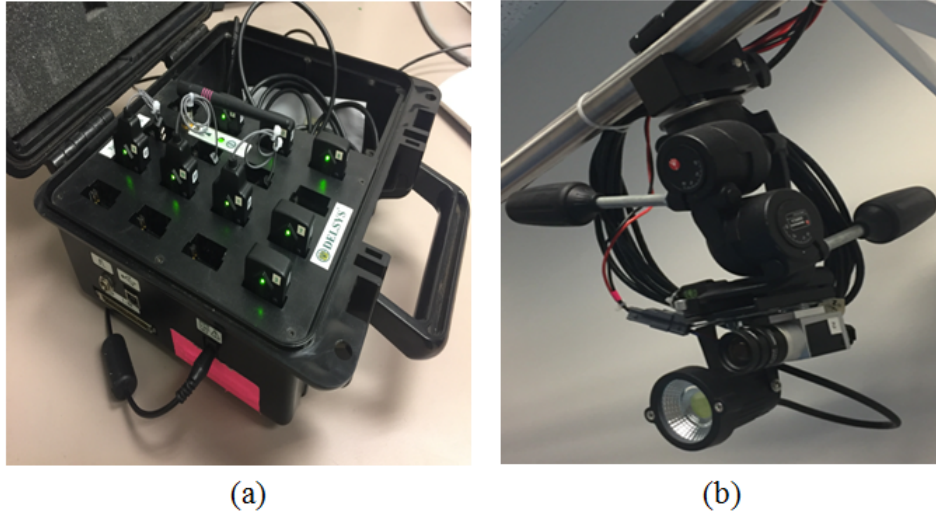


Figure 3.2: (a) Trigno and (b) high speed camera obtained from the Department of Kinesiology at Lakehead University

3.2 Experimental Validation

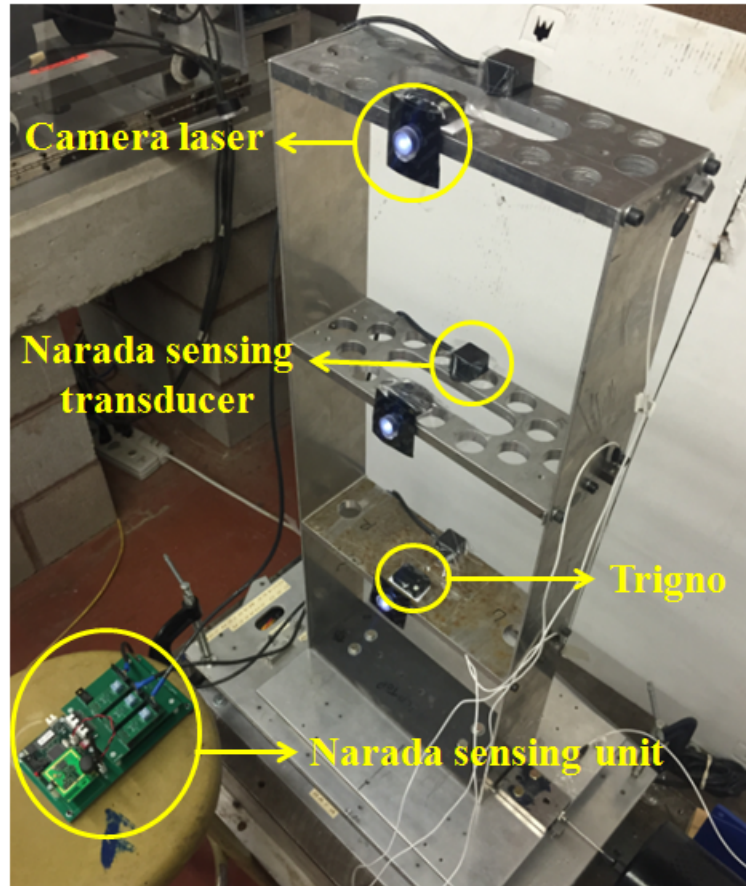


Figure 3.3: Narada, Trigno and Camera attached to the experimental model

Before implementing data compression techniques, validation studies are first conducted on a 3-DOF experimental model as shown in Fig. 3.3 to check the adequacy of the Narada sensors. The objective of these experiments is to evaluate the performance of Narada with a well-calibrated high speed camera, and another wireless sensor, namely Trigno. A single channel sensor is placed at the middle of each floor, where the sampling frequencies are set to be 200 Hz for Narada, 148 Hz for Trigno and 60 Hz for the camera. With the aid of a control system and shake table, impact and random forces are subjected to validate capability of monitoring the 3-DOF model.

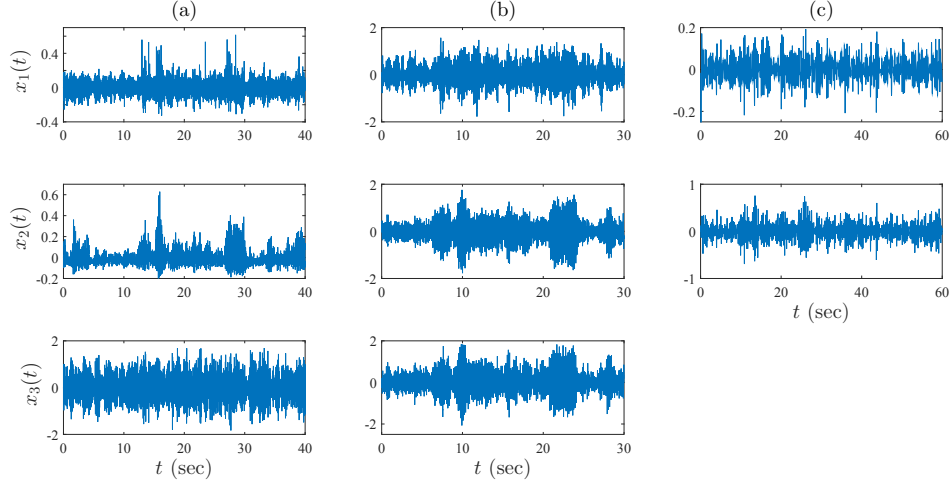


Figure 3.4: Time histories of floor responses measured by (a) Narada, (b) Trigno and (c) camera obtained from the impact force test

The time histories and Fourier spectra of floor responses obtained from the impact test are illustrated respectively in Fig. 3.4 and Fig. 3.5. Similar results are respectively shown in Fig. 3.6 and Fig. 3.7 under random force excitation. It is clear that the performance of Narada sensor is equivalent to Trigno for all three structural modes. It may be noted that camera could not capture higher frequencies due to its low sampling frequency used in this application, however the first mode is correctly captured and compared for all three sensors. A summary of frequency analysis obtained from all tests by Narada, Trigno and the high speed camera is illustrated in Table 3.1. In brief, Narada, Trigno and the high speed camera have shown great performance in monitoring low frequency systems. In fact, the Fourier spectra of the floor measurements prove that the extracted natural frequencies, as shown in Table 3.1, are very similar to the theoretical natural frequencies of the model which are 7, 14 and 24 Hz, respectively. The results prove that the Narada sensors are capable of measuring vibration data even with low sampling rate and suitable for the proposed research.

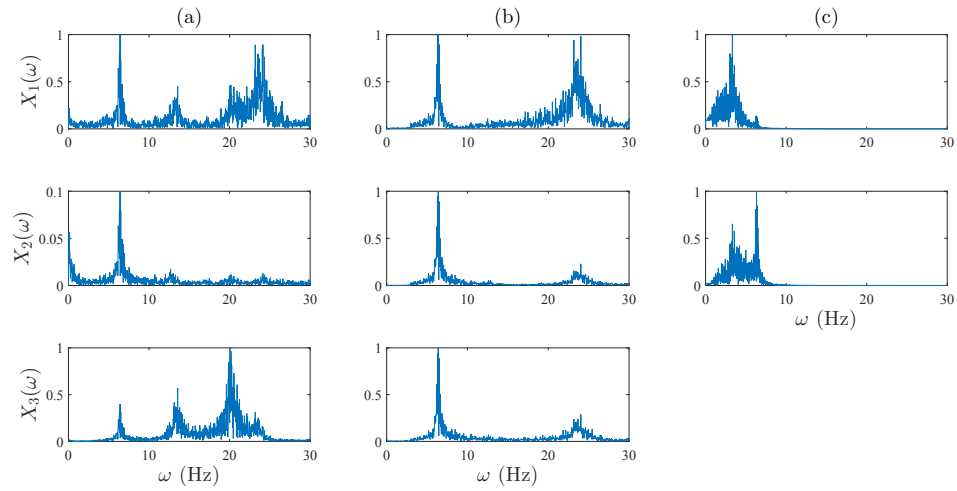


Figure 3.5: Fourier spectra of floor responses measured by (a) Narada, (b) Trigno and (c) camera obtained from the impact force test

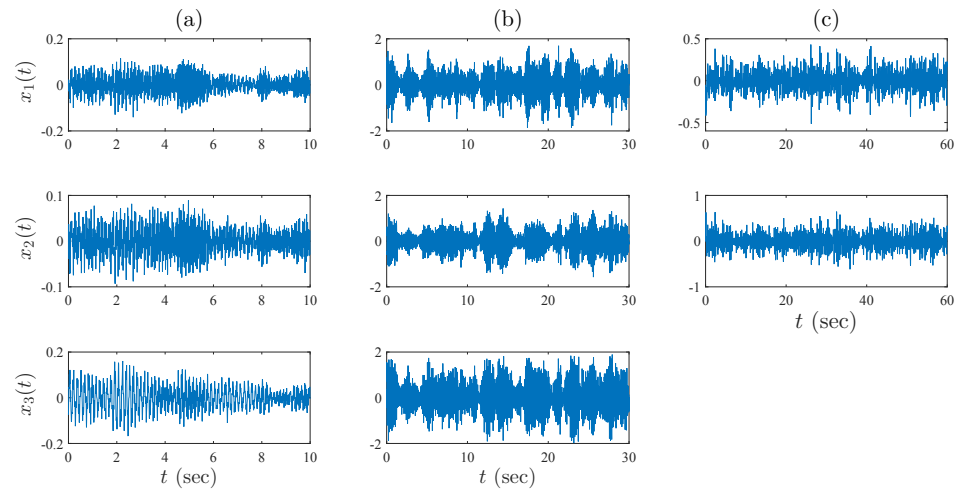


Figure 3.6: Time history of floor responses measured by (a) Narada, (b) Trigno and (c) camera obtained from the random force test

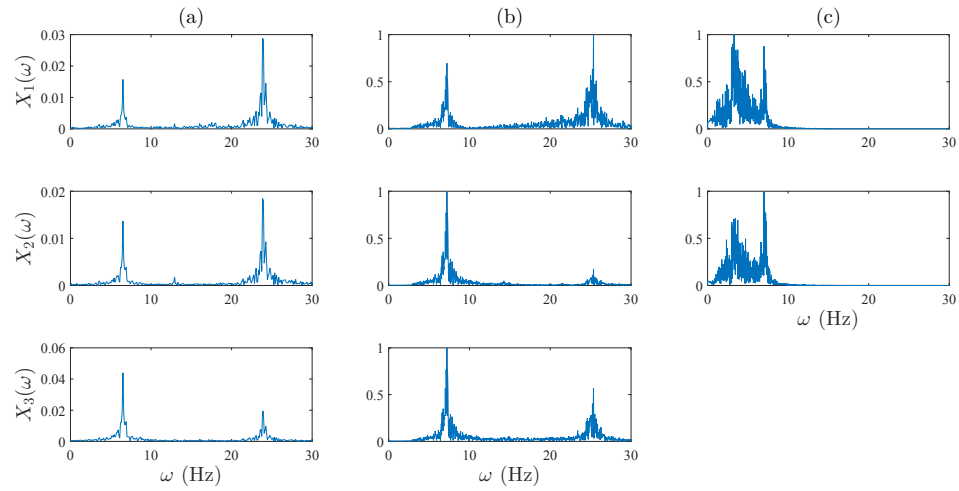


Figure 3.7: Fourier spectra of floor responses measured by (a) Narada, (b) Trigno and (c) camera obtained from the random force test

Table 3.1: Summary of frequency analysis obtained from three different sensors under a wide range of excitation

Type of test	Narada			Trigno			Camera
	ω_1	ω_2	ω_3	ω_1	ω_2	ω_3	ω_1
impact	6.4	13.6	24.1	6.4	12.6	24	6.3
random	6.5	12.9	24	7.2	14.2	24.3	7

Chapter 4

Numerical Studies

This chapter presents the results and discussions of data compression techniques proposed in this thesis using a wide range of numerical models. The proposed data compression techniques are then validated using the undersampled data and the accuracy of data reconstruction is evaluated through system identification.

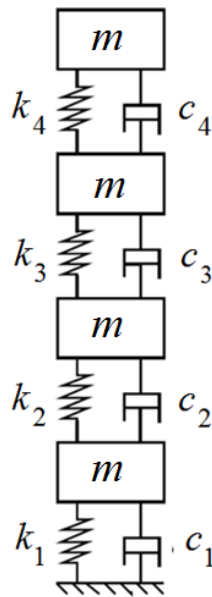


Figure 4.1: 4-DOF Model

4.1 4-DOF Model

A 4-DOF mass-spring-damper system as illustrated in Fig. 4.1 [24] is utilized in this study. A mass of 1 kg and stiffness of $k_1 = k_3 = 7000$ N/m and $k_2 = k_4 = 8000$ N/m

are used to simulate the model. A random base excitation is subjected to the model to simulate floor responses. Each floor measurement is simulated for 30 seconds with a sampling frequency of 50 Hz (i.e., 1500 samples of data). Time histories of floor responses obtained from the 4-DOF model are shown in Fig. 4.2 which are used to compare the relative performances of LNM and DCT.

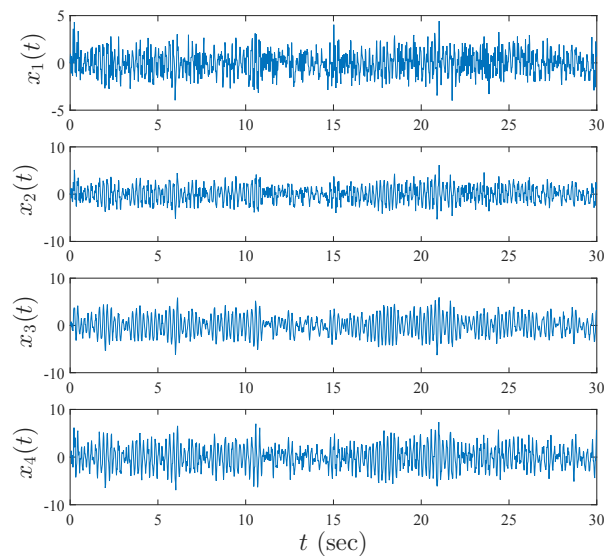


Figure 4.2: Time histories of floor responses obtained from the 4-DOF model

LNM is first used to compress the data of first and fourth floors using a compression rate of 20% and 50%, respectively. For example, Fig. 4.3 and Fig. 4.4 the compressed data and reconstructed signal of first floor response whereas Fig. 4.5 and Fig. 4.6 show similar results of the fourth floor. Data compression of 20% results in 1200 samples of data out of 1500 data points, while a rate of 50% results in 750 samples. A compression rate of 20% has shown high accuracy of data reconstruction for both floors as illustrated in Fig. 4.3 and Fig. 4.5, where $x(t)$, $y(t)$ and $x_r(t)$ are original, compressed and reconstructed signals respectively. Reconstructed Fourier spectrum is almost same as original measurements which indicate a sign of reliable

recovery of compressed data. However, the performance of LNM with 50% compressed data reveals lesser accuracy as shown in Fig. 4.4 and Fig. 4.6, respectively.

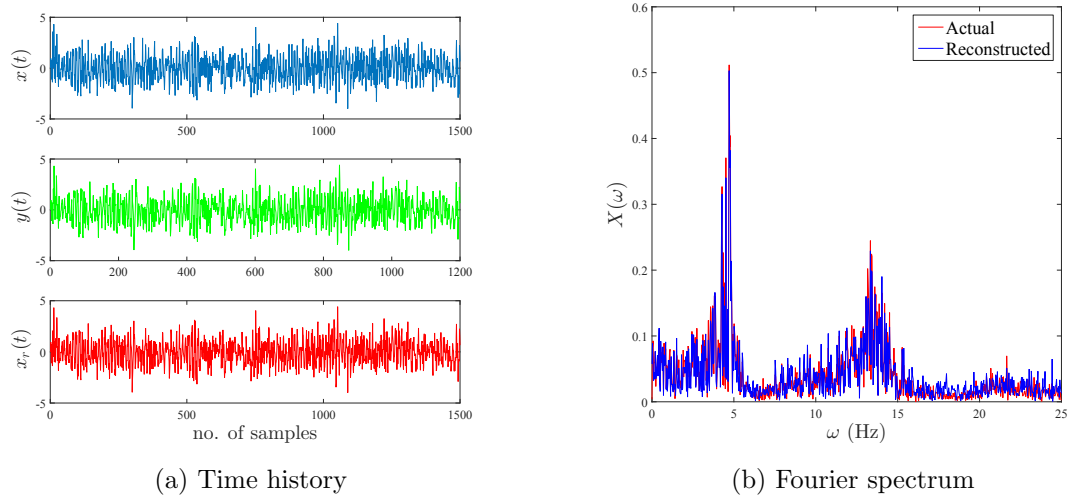


Figure 4.3: 20% data compression of first floor response by LNM

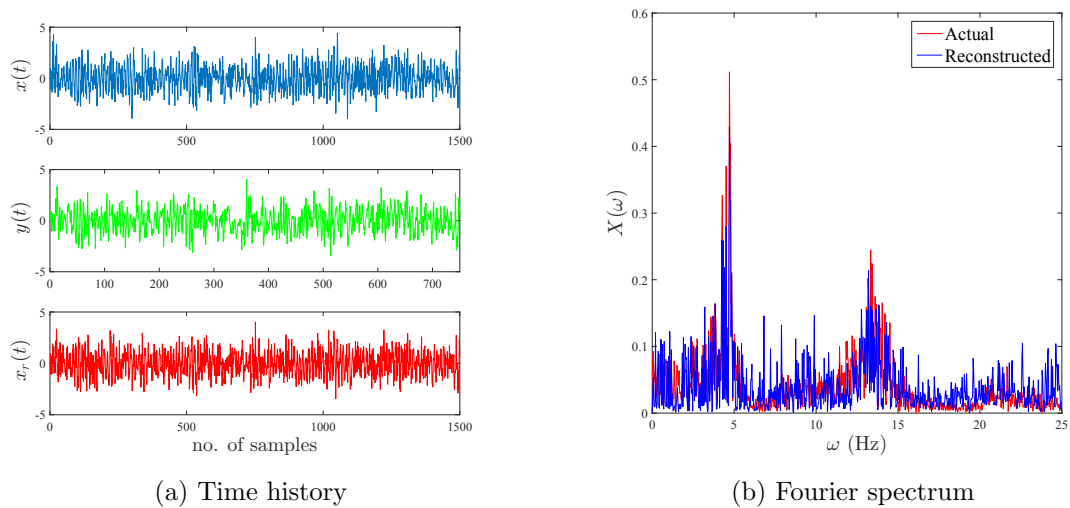


Figure 4.4: 50% data compression of first floor response by LNM

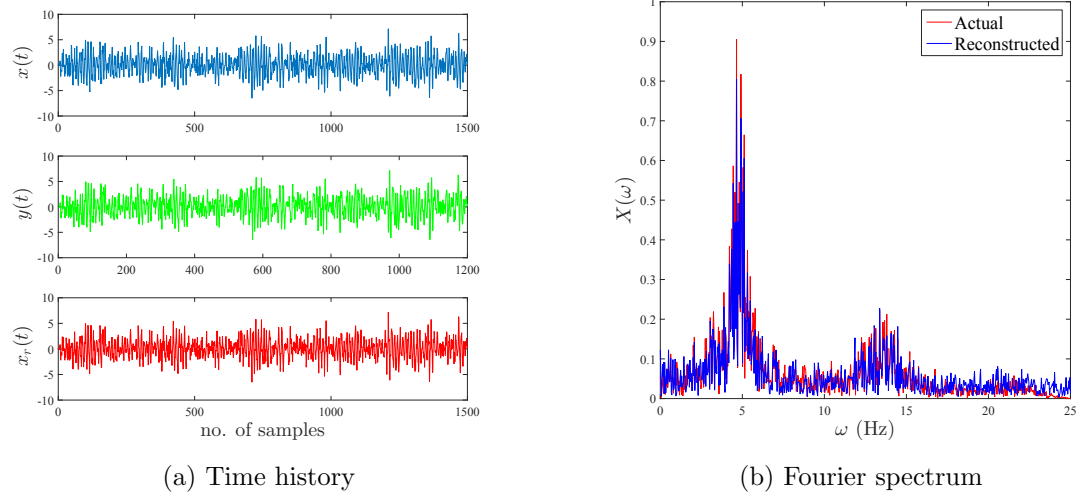


Figure 4.5: 20% data compression of fourth floor response by LNM

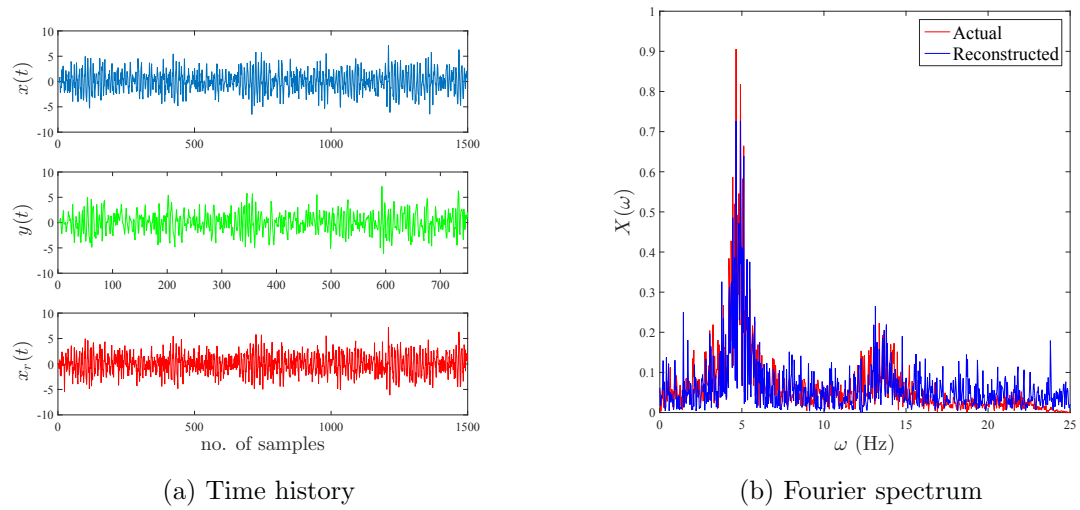


Figure 4.6: 50% data compression of fourth floor response by LNM

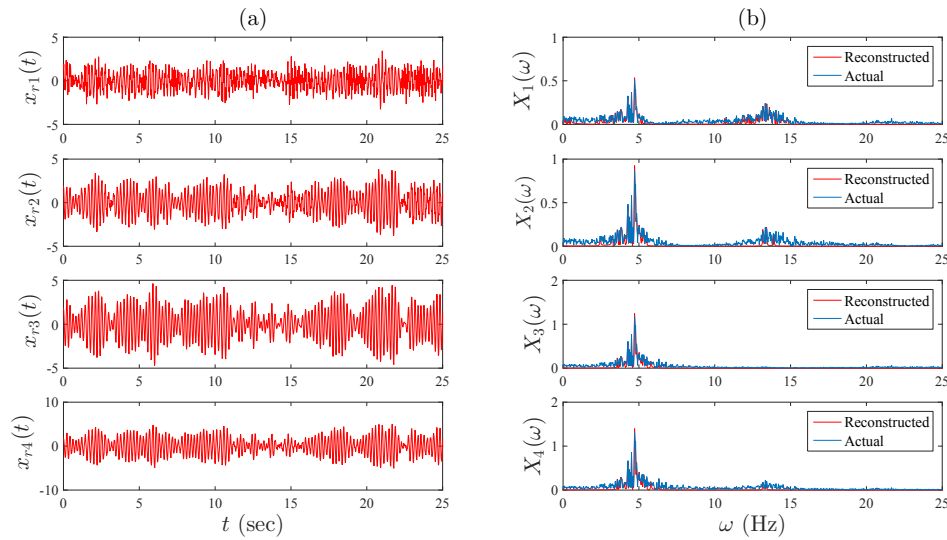


Figure 4.7: (a) Time histories and (b) Fourier spectrum of floor responses obtained from reconstructed data using DCT

In order to show its performance in data recovery, DCT is performed with 12% threshold level of the maximum DCT coefficients in order to discard values below the level, which is approximately equivalent to 40% data compression. In Fig. 4.7, time histories and Fourier spectrum of floor response show high accuracy of data reconstruction. Since the size of a signal includes some notion of its strength, the mathematical concepts of the norm is used to quantify the observed signals, as the norm is a function that assigns length or size to each vector. Therefore, the accuracy of data reconstruction by DCT can be determined by comparing the size of the norm between the original and reconstructed data. The norm of a data set can be used to formulate the convex-hull [39] where it is possible to measure the norm for different sets of data as shown in Fig. 4.8. The data is triangulated to apply the convex-hull in order to show the norm boundaries of the original and reconstructed data. As shown in Table 4.1, the boundaries of the original and reconstructed data in each floor signal reflects the accurate data reconstruction applied by DCT in terms of comparing their

norm sizes. This numerical study proves that both LNM and DCT may be considered as a potential data compression tool to improve the capability of handling big data in SHM applications.

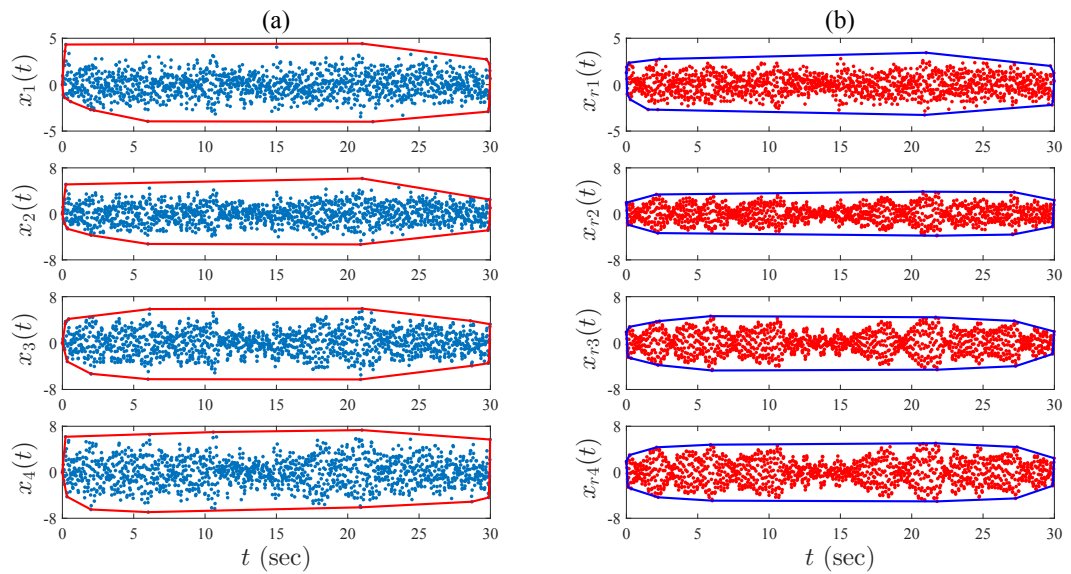


Figure 4.8: Convex hull of the data norm: (a) original data and (b) reconstructed data

Table 4.1: Size of the norm of the original and reconstructed data by DCT

Floor #	1	2	3	4
$x(t)$	23.21	34.74	45.37	51.81
$x_r(t)$	20.91	30.94	42.17	47.13

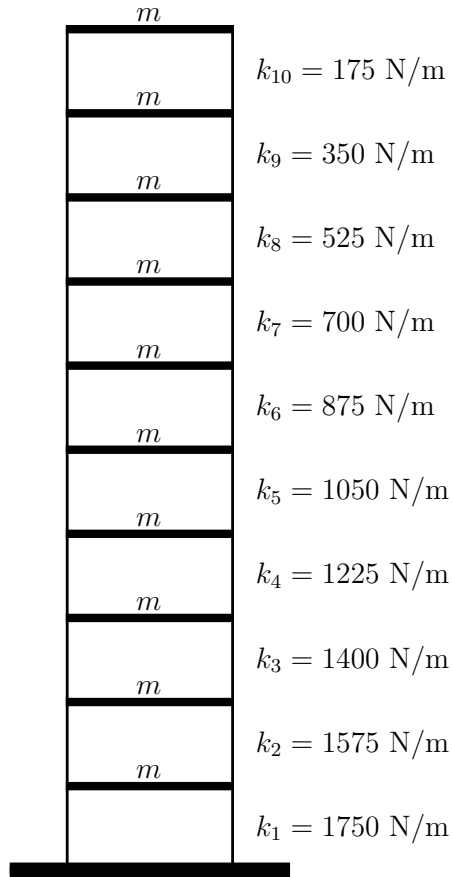


Figure 4.9: 10-DOF Model

4.2 10-DOF Model

In this section, a simulation study is performed to validate both methods and compare their results of a 10-DOF model as illustrated in Fig. 4.9. The lumped mass of each floor is assumed to be 1 kg, the damping is assumed to be 2% critical in all modes, and the stiffness of each floor is shown in Fig. 4.9. Both data compression methods are applied to the time history of each floor as simulated in Fig. 4.10. Fourier spectra of the simulated floor responses are shown in Fig. 4.11. TFBSS is first employed on the simulated responses and the resulting Fourier spectra of identified sources are shown in Fig. 4.12. With mono-component nature of sources, it is clear that TFBSS

is able to accurately separate modal responses of original data.

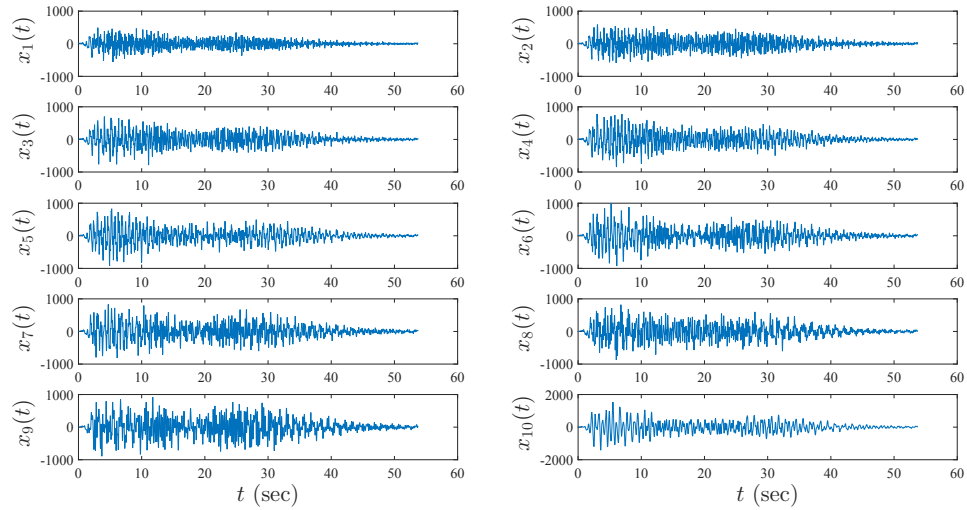


Figure 4.10: Time histories of floor responses obtained from the 10-DOF model

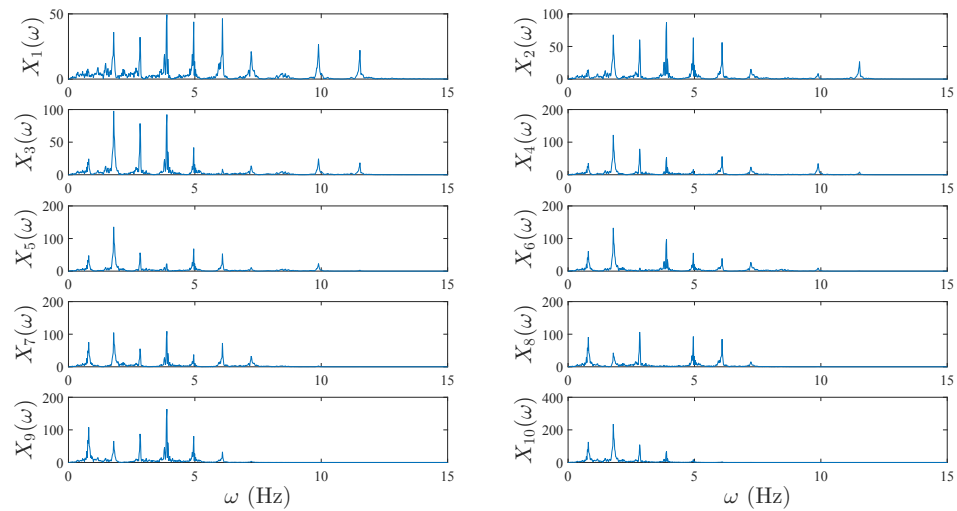


Figure 4.11: Fourier spectra of floor responses obtained from the 10-DOF model

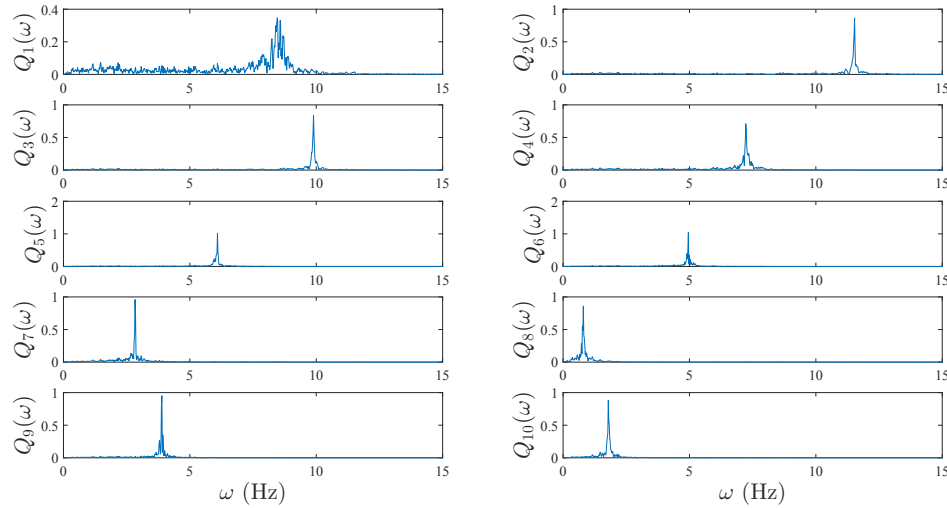


Figure 4.12: Fourier spectra of modal responses obtained from TFBSS using the original data

In order to compare the performance of LNM and DCT, TFBSS is utilized to conduct modal identification using reconstructed data. The sources of the original and reconstructed data are then analyzed to compare both proposed methods. LNM is first performed on data with 10% data compression. The resulting time histories and Fourier spectra of reconstructed signals are respectively illustrated in Fig. 4.13 and Fig. 4.14. Fourier spectra of identified sources of TFBSS using LNM assisted reconstructed signals are shown in Fig. 4.15 which reveals significant mode-mixing in the modal responses. These results also indicate inefficiencies of retaining correct modal information from the data reconstructed by LNM.

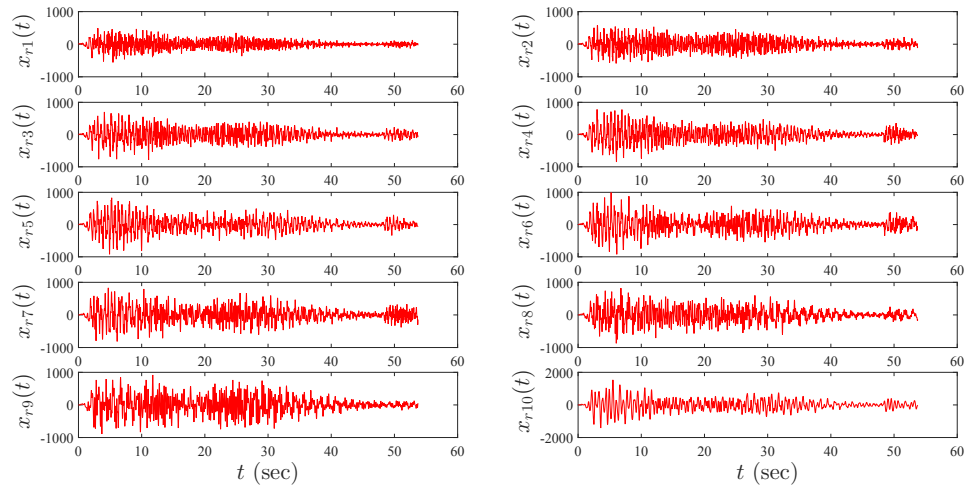


Figure 4.13: Time histories of floor responses obtained from the reconstructed data by LNM

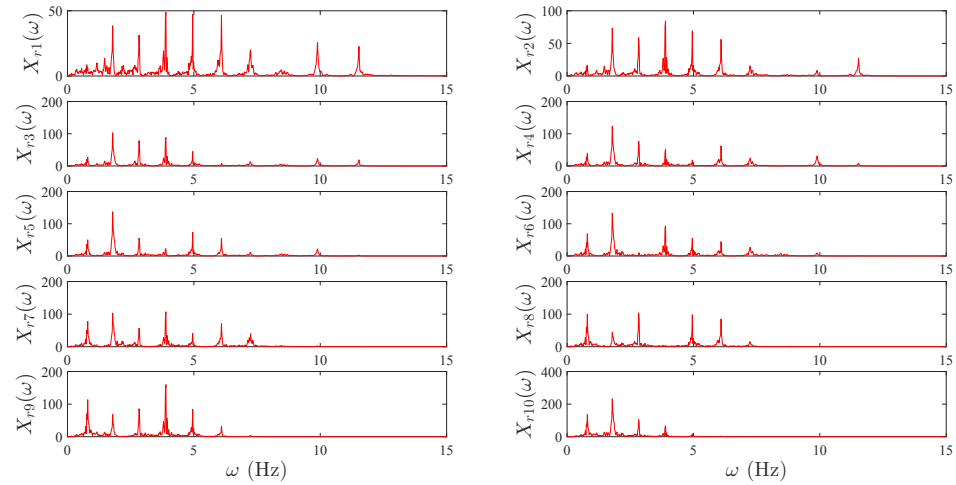


Figure 4.14: Fourier spectra of floor responses obtained from the reconstructed data by LNM

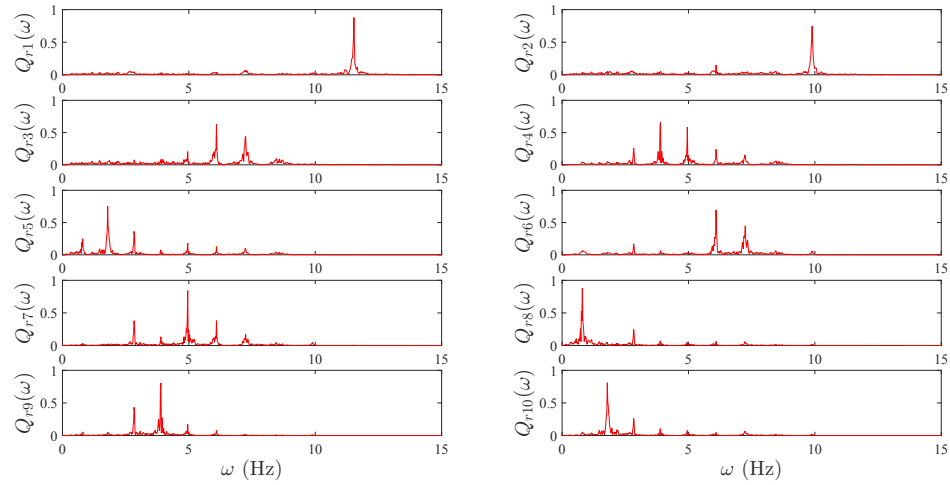


Figure 4.15: Fourier spectra of modal responses obtained from TFBSS using the reconstructed data by LNM

While using DCT, a threshold rate of 12% is adopted to discard up to 40% of the original data. Time histories and Fourier spectra of the reconstructed signals using DCT are respectively shown in Fig. 4.16 and Fig. 4.17, while Fourier spectra of identified sources obtained from DCT assisted reconstructed signals are shown in Fig. 4.18. From Fig. 4.18, it is clear that all sources resulting from DCT-assisted reconstructed data are mono-component in nature. Unlike LNM, it is possible to identify all modal responses from the reconstructed data offered by DCT. Finally, the identified frequencies of the modal responses obtained from original data and DCT-assisted reconstructed data are summarized in Table 4.2.

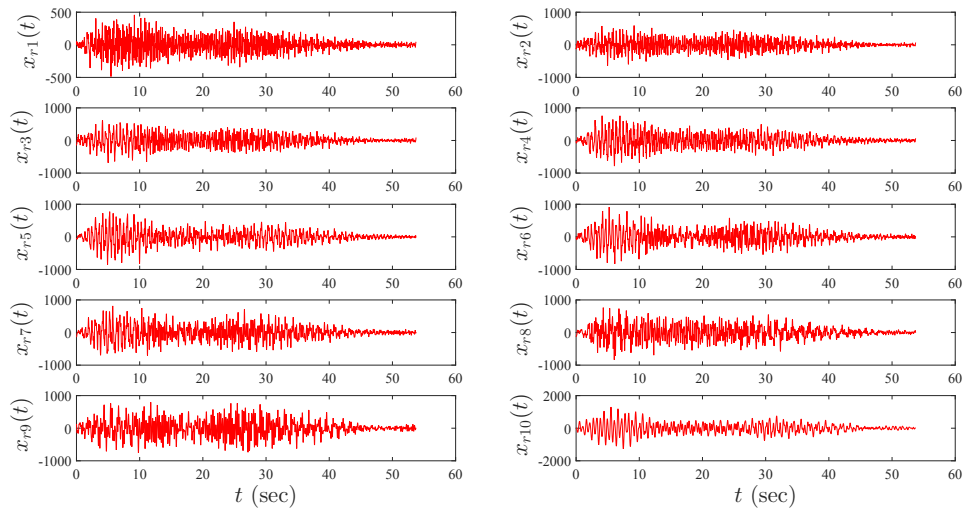


Figure 4.16: Time histories of floor responses obtained from the reconstructed data by DCT

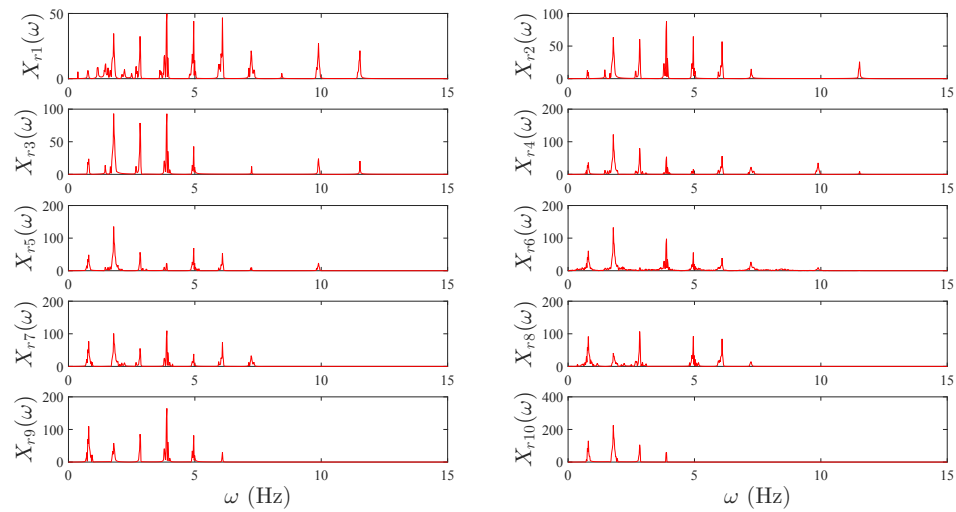


Figure 4.17: Fourier spectra of floor responses obtained from the reconstructed data by DCT

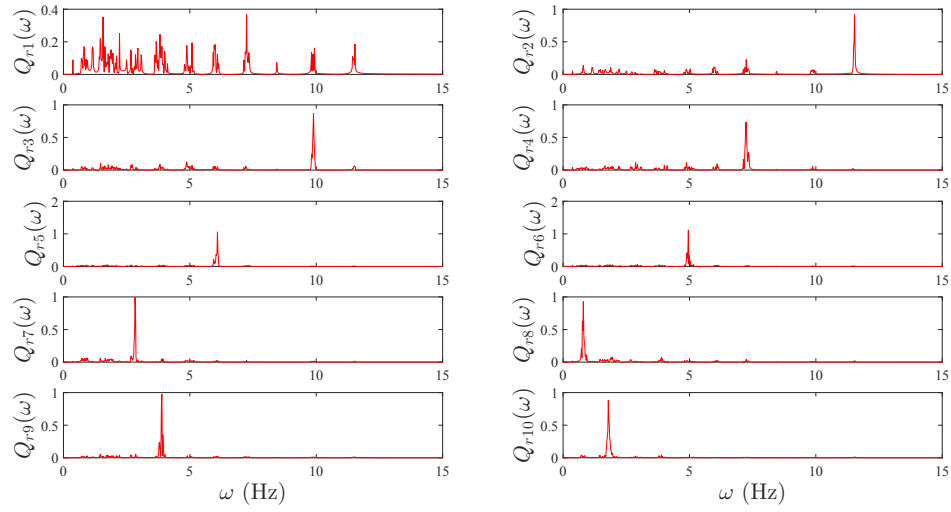


Figure 4.18: Fourier spectra of modal responses obtained from TFBSS using the reconstructed data by DCT

Table 4.2: Identification results of the 10-DOF model using DCT method

ω (Hz)	ω_1	ω_2	ω_3	ω_4	ω_5	ω_6	ω_7	ω_8	ω_9	ω_{10}
Actual	0.80	1.79	2.83	3.89	4.96	6.09	7.23	8.46	9.89	11.53
DCT	0.80	1.79	2.83	3.89	4.96	6.09	7.29	8.44	9.89	11.53

Chapter 5

Experimental and Full-scale Validation

In this chapter, the proposed data compression techniques are validated through different experimental models and a full-scale structure. The properties of the experimental models are carefully chosen to reflect true dynamic behavior of civil structures. These models are subjected to either base excitation or random floor excitation and the measured data are collected through wireless or wired sensors.

This experimental work includes two lab-scale building models (i.e., model A and model B) and a cantilever beam, whereas a long-span bridge located in Thunder Bay is utilized for full-scale validation. Model A is defined as a 3-DOF model with a height of 80 cm which was developed at Lakehead University. Model B is another 3-DOF model with a height of 2 m and different mass and stiffness distribution that was developed at IIT Kanpur during the candidate's internship in India.

5.1 Model A

The masses of this model, shown in Fig. 5.1, from first floor to top floor are 3.2, 1.1 and 0.656 kg, respectively [38]. The two-sided columns are made of aluminium with a mass of 0.718 kg, and the dimensions are 776.5 mm (height), 107.2 mm (width), 3.08 mm (thickness), and 257.1 mm (height) between floors. The model is placed on a shake table connected to a modal shaker that can generate random or any pre-determined forces. As shown in Fig. 5.1, three sensing transducers are placed at each

floor and connected to the sensing unit which wirelessly communicates with Narada sensors on a computer through the base station. The model is excited by random shaking for 30 seconds using a control system attached to the modal shaker. Two different approaches of under-sampling are performed: (a) explicit and (b) implicit. In explicit mode of undersampling, the data is first sampled with adequate sampling frequencies and then it is randomly undersampled to form a database for the data reconstruction. In case of implicit approach, the data is undersampled within the sensor level which is then reconstructed using the proposed method.

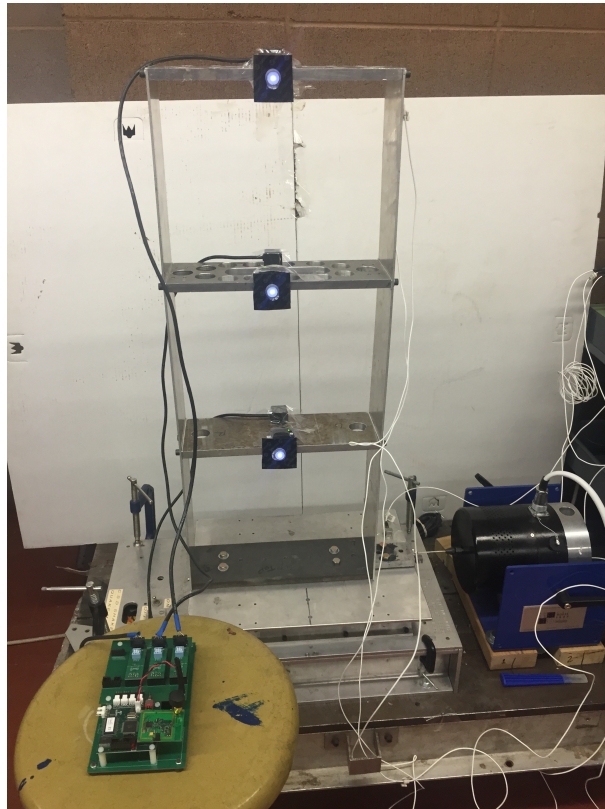


Figure 5.1: Model A

5.1.1 Explicit Data Compression

The data is first collected with a sampling frequency of 200 Hz. The observed data is used for compression through CS to under-sample the original signals, and then

these signals are recovered from fewer measurements considering certain rates of data compression (i.e., 20%, 40% and 60%).

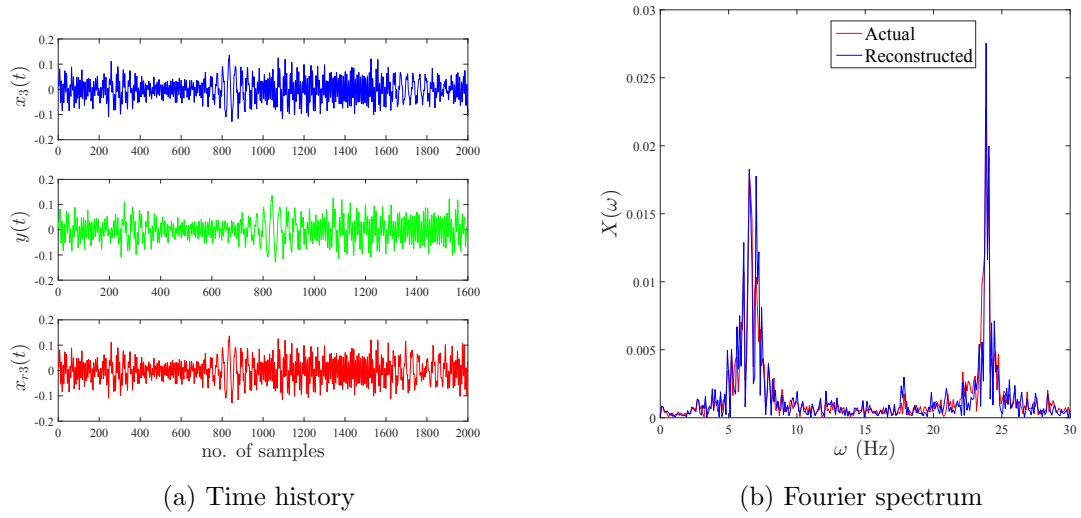


Figure 5.2: 20% data compression of third floor by LNM

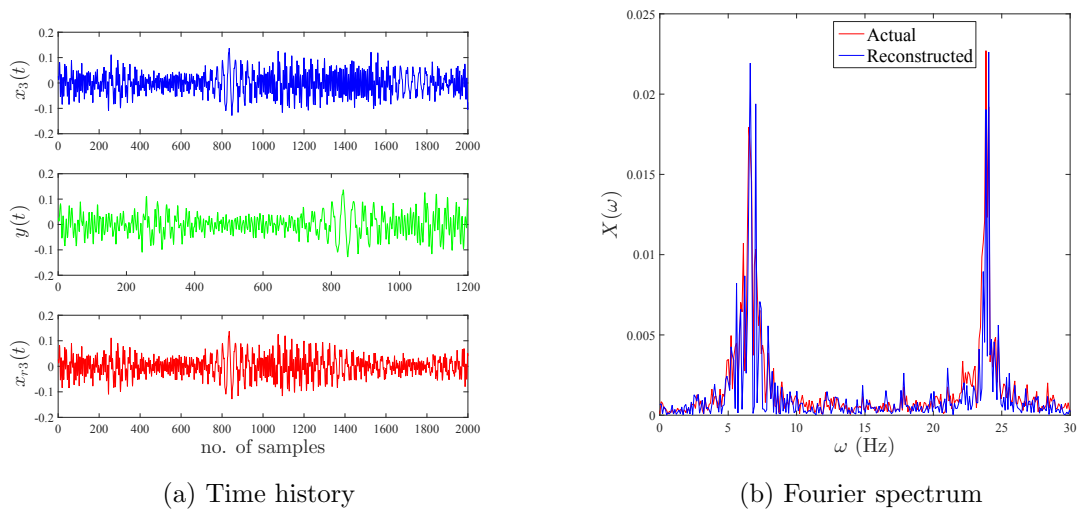


Figure 5.3: 40% data compression of third floor by LNM

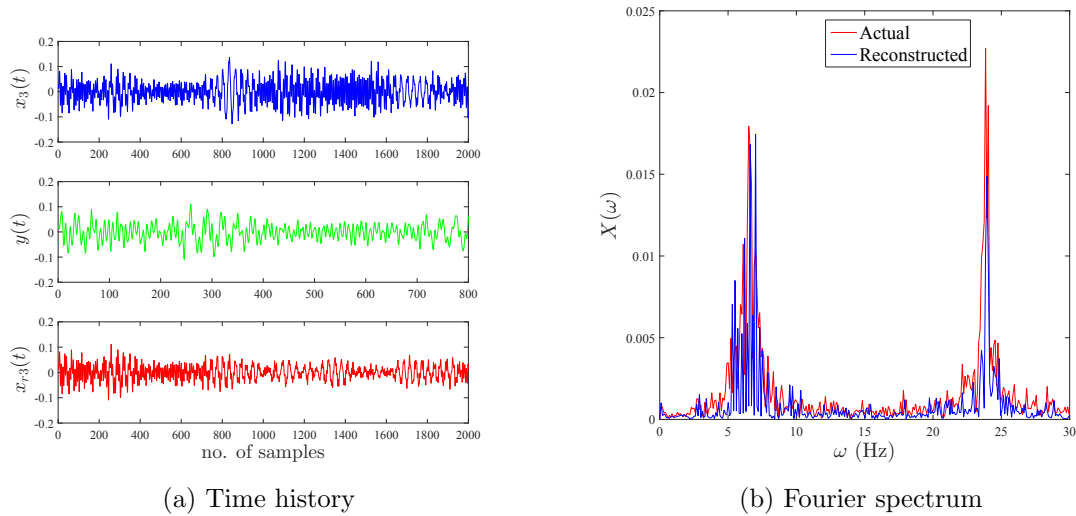


Figure 5.4: 60% data compression of third floor by LNM

As shown in Fig. 5.2 (a), the observed data is reduced to produce a compressed signal $y(t)$ that contains 1600 random sampled data points under 20% data compression (i.e. $2000 \times 0.8 = 1600$). The resulting undersampled data is reconstructed to recover the signal with exactly same number of original samples $x_r(t)$. Fourier spectrum of actual and reconstructed signals are generated and compared to show the relative efficiency of the proposed data compression technique. Data compressing of 40% and 60% are also applied to the set of data of the third floor as illustrated respectively in Fig. 5.3 and Fig. 5.4. It is clear that compression rates of 20% and 40% show reliable data recovery, while in a compression rate of 60% reconstructed signals seems to be insufficiently accurate.

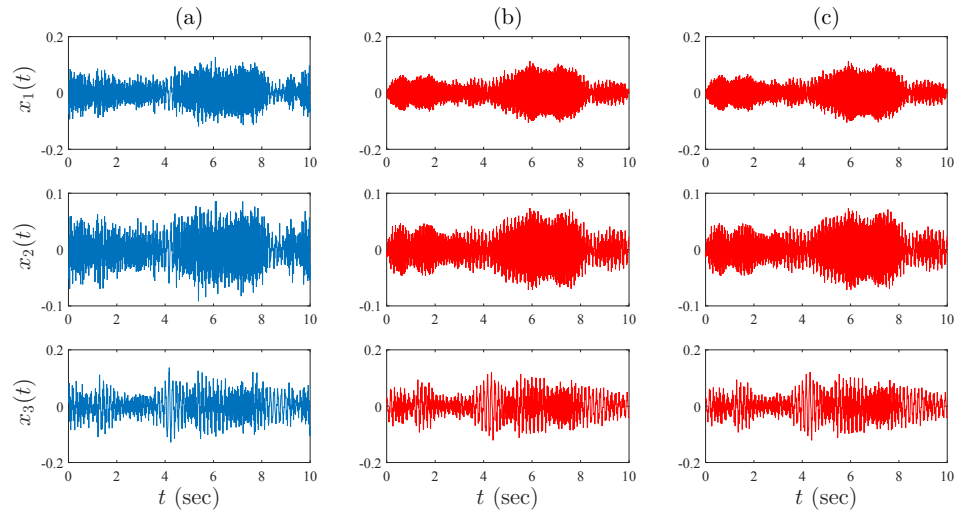


Figure 5.5: Time histories of floor responses obtained from (a) original data, (b) reconstructed data by LNM and (c) reconstructed data by DCT

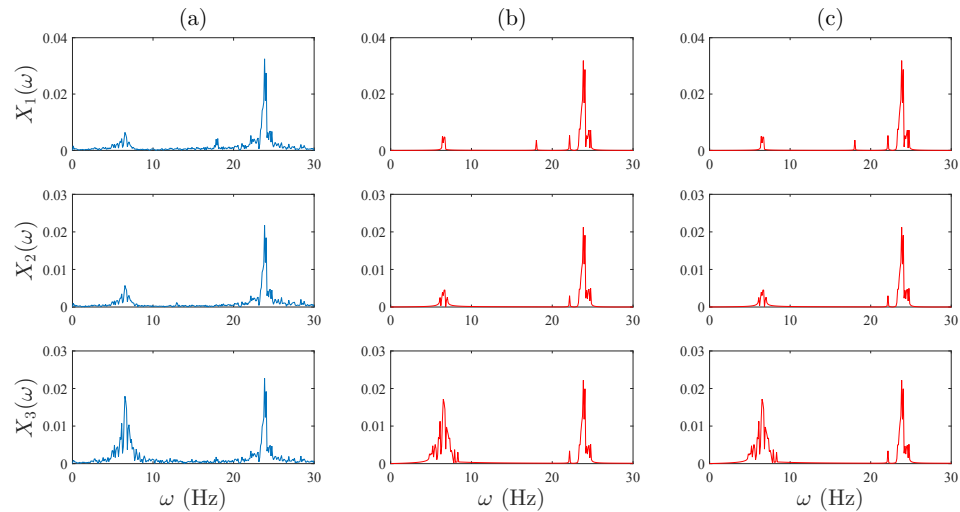


Figure 5.6: Fourier spectra of floor responses obtained from (a) original data, (b) reconstructed data by LNM and (c) reconstructed data by DCT

In order to compare the performance of LNM and DCT, TFBS is applied on the original data and the identified modal frequencies are compared with LNM and DCT-assisted reconstructed data. The plots of original and reconstructed data using both methods are shown in column (a), (b) and (c) of Fig. 5.5 and Fig. 5.6, respectively. Fourier spectra of modal responses obtained from the original and reconstructed data

using TFBSS are plotted in Fig. 5.7. A compression rate of 40% is considered for LNM, and a threshold level of 12% of the maximum coefficient in DCT is set to be approximately an equivalent percentage to the 40% data compression. Compared to the Fourier spectrum of original modal responses shown in Fig. 5.7, both methods clearly present the modes separately; however, the quality of source separation is better in DCT as it indicates the three modes, while in LNM it only indicates two modes.

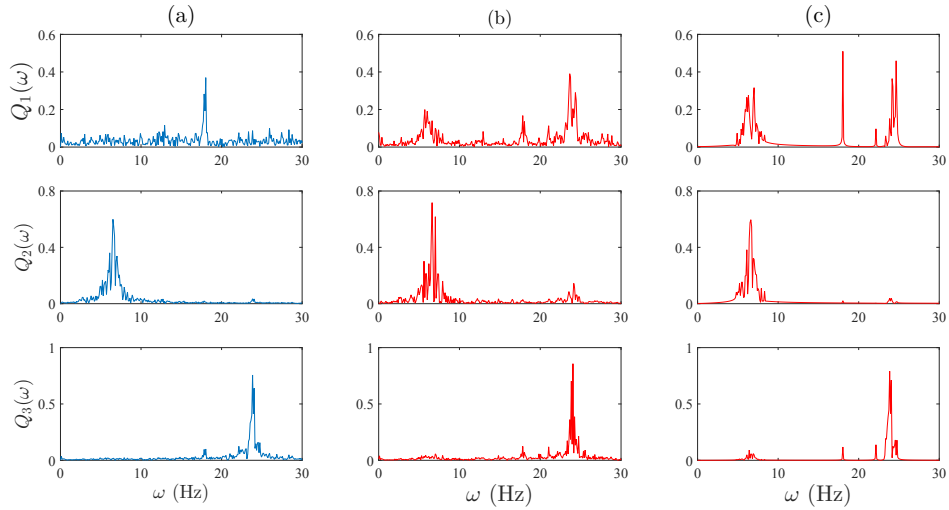


Figure 5.7: Fourier spectra of modal responses using TFBSS obtained from (a) original data, (b) reconstructed data by LNM and (c) reconstructed data by DCT

5.1.2 Implicit Data Compression

A real case of CS application is considered in this section where the collected data is assumed to be under-sampled through the wireless sensors. Therefore, only reconstruction process is required to perform data recovery. Two tests with reduced sampling frequencies (f_s), as illustrated in Table 5.1, are conducted using Narada sensor on Model A, where the model is impacted by a hammer.

Table 5.1: Details of implicit data compression

Experiments	f_s (Hz)	No. of Samples	Duration (sec)
Test 1	50	1250	25
Test 2	100	2500	25

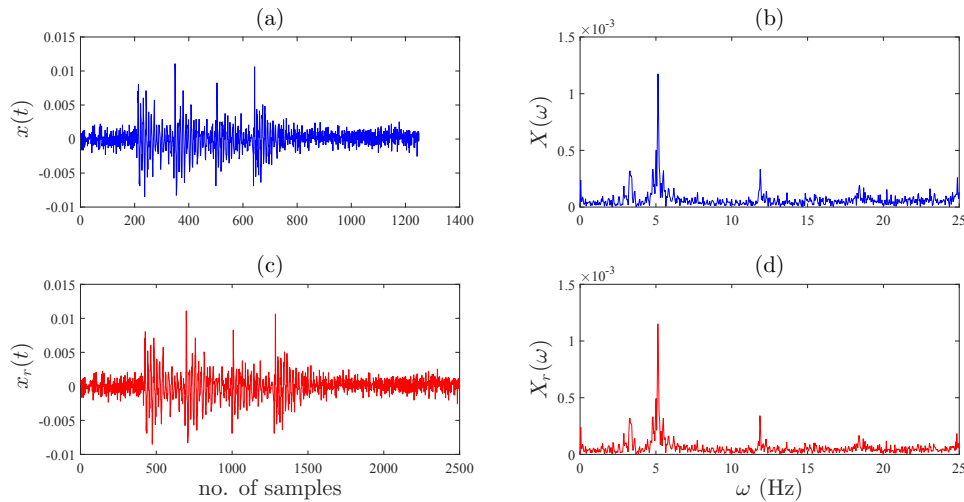


Figure 5.8: (a) Time history of Test 1, (b) Fourier spectrum of Test 2, (c) Time history of the reconstructed signal of Test 1 by LNM, and (d) Fourier spectrum of reconstructed signal of Test 1 by LNM

A single wireless sensor is located at the middle of the third floor to collect data of Test 1 and Test 2, where the signal of Test 1 is reconstructed with the same number of samples of Test 2 (i.e., 2500 samples). Fourier spectrum obtained from Test 2 and reconstructed data of Test 1 are generated to compare the performance of data reconstruction. The objective of this study is to investigate whether it is possible to set lower sampling frequency for testing and simply apply LNM to reconstruct the signals as desired. As shown in Fig. 5.8(a), time history of floor response obtained from Test 1 is already compressed implicitly. The signal is then reconstructed by LNM as illustrated in 5.8(c). Fourier spectrum obtained from Test 2 (i.e., data collected with $f_s = 100$ Hz) and the reconstructed signal by LNM are respectively shown in Fig. 5.8(b) and Fig. 5.8(d) which shows significant promise of LNM in data

reconstruction. The collected data of Test 1 is now used to apply data compression through DCT, as shown in Fig. 5.9. The threshold is applied with a rate of 10% of the maximum DCT energy in order to discard up to 40% of the original data, and then IDCT is applied for reconstruction. It is clear that data compression using DCT achieves sufficient rates and accuracy of data compression without losing significant features of the signals.

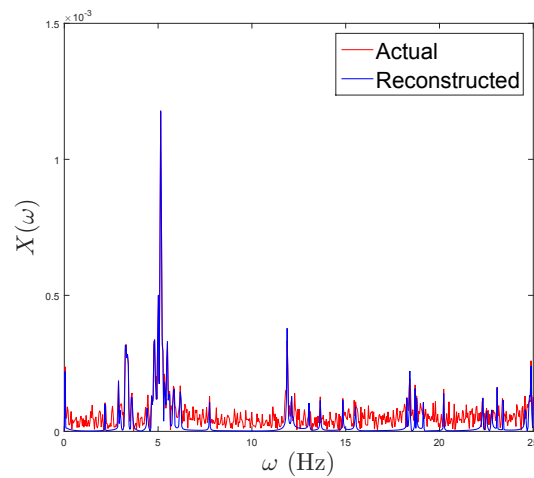


Figure 5.9: Fourier spectrum of floor responses obtained from Test 1 using DCT

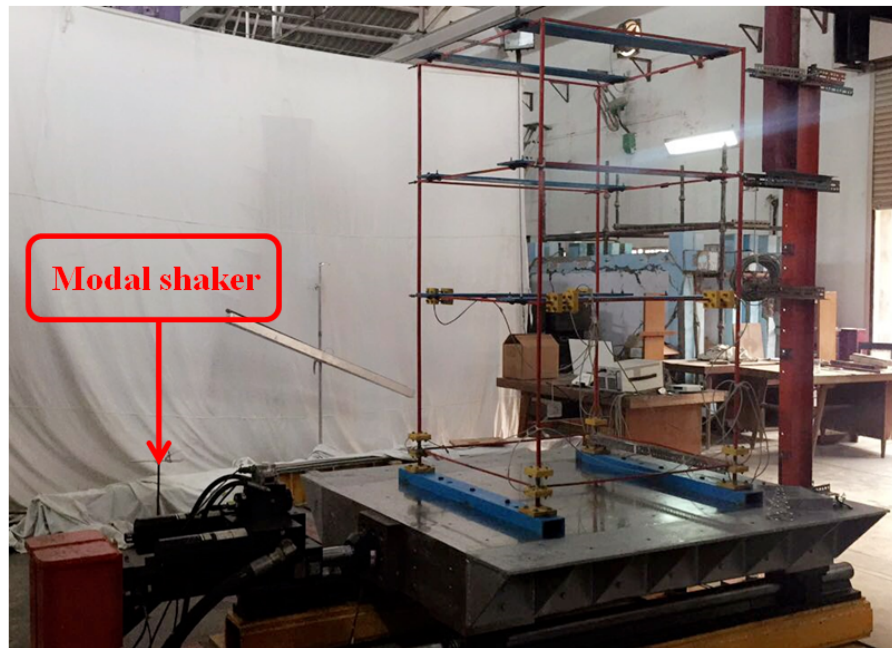


Figure 5.10: Model B

5.2 Model B

Model B is defined as a 3-DOF experimental model that is attached to a modal shaker, as shown in Fig. 5.10. This model belongs to the laboratory of structural engineering at IIT Kanpur in India which was tested during the candidate's research internship at IIT Kanpur. The servo-hydraulic shake table is supplied with a uni-axial actuator that can simulate real earthquake motions, and can be utilized for seismic verification of large-scale structural systems. The shake table platform measuring is medium sized with 1.2×1.8 m, and it is powered by 50 kN - 150 mm MTS servo-hydraulic actuator which can generate velocities in the range of 1.5 m/s and acceleration of $5g$. The weight of table is 8 kN and maximum payload of 40 kN. Maximum displacement is 75 mm and frequency range is up to 50 Hz.

This model has been tested with white noise and ground motions subjected by the shaker and dynamically monitored using wired sensors with a sampling frequency of 1000 Hz. Six accelerometers have been placed on both ends of one span of each floor, as highlighted in Fig. 5.11. The time histories and Fourier spectra of floor responses are generated from the observed data in order to extract the model's dynamical properties before and after a discrete damage in the model. In this way, the performance of the proposed data compression is checked with the data containing damage signature. Two different excitations (i.e., random and base excitation) are considered.

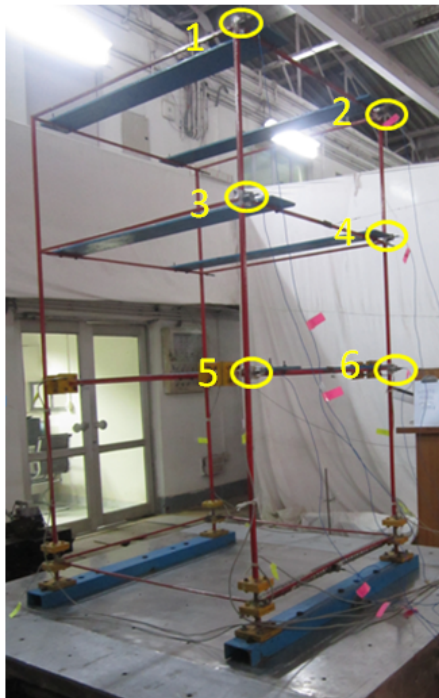


Figure 5.11: Location of six accelerometers placed on Model B

5.2.1 Baseline (w/o any damage)

The performance of this experimental model before damage is tested with white noise and ground motions, and then data compression using DCT is applied to the

observed data obtained from both tests. First, as white noise of 0.05 g is subjected by the model shaker, time histories and Fourier spectra of floor responses obtained from the experimental model are respectively presented in Fig. 5.12 and Fig. 5.13. Second, ground motion test is considered to check the performance of this experimental model under base excitation. The time histories and Fourier spectra of floor responses obtained from the model are respectively presented in Fig. 5.14 and Fig. 5.15. The performance of DCT is illustrated in Fig. 5.16 and Fig. 5.17 for the white noise test, while Fig. 5.18 and Fig. 5.19 present the data compression through DCT for the ground motion test.

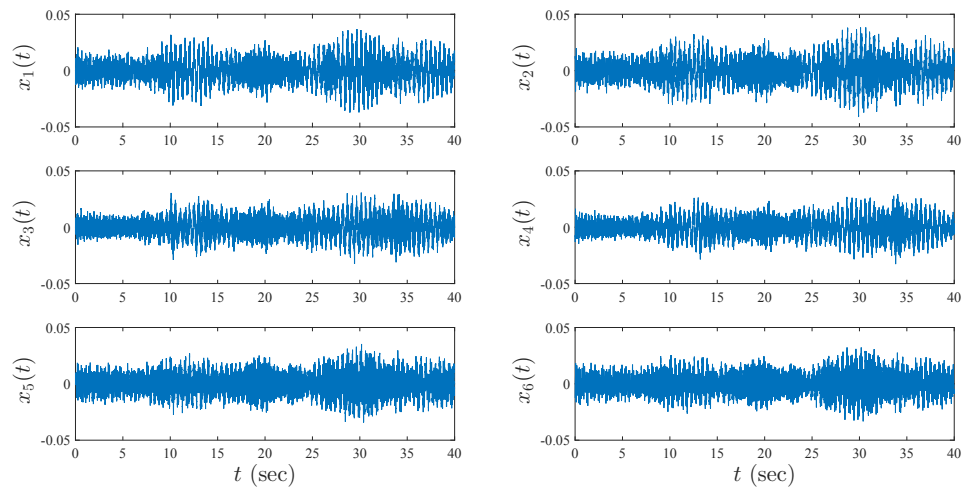


Figure 5.12: Time history of floor responses obtained from Model B before damage (white noise)

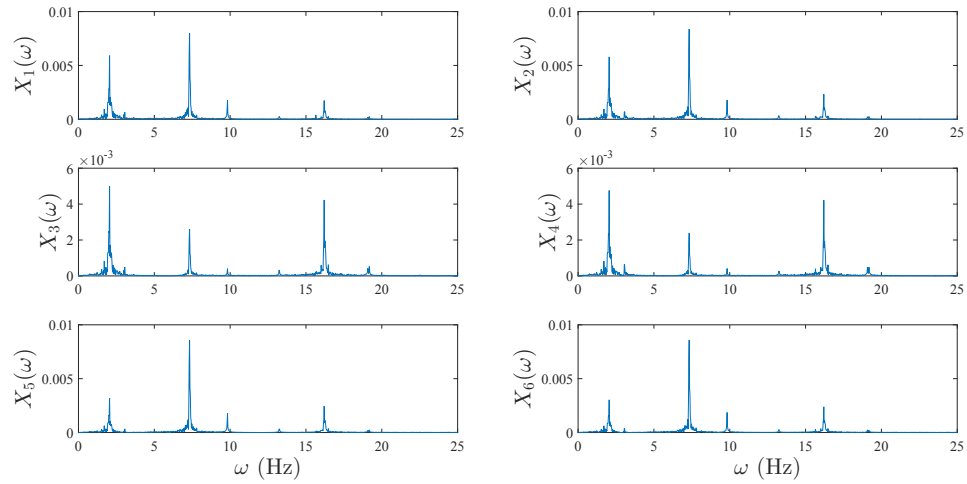


Figure 5.13: Fourier spectrum of floor responses obtained from Model B before damage (white noise)

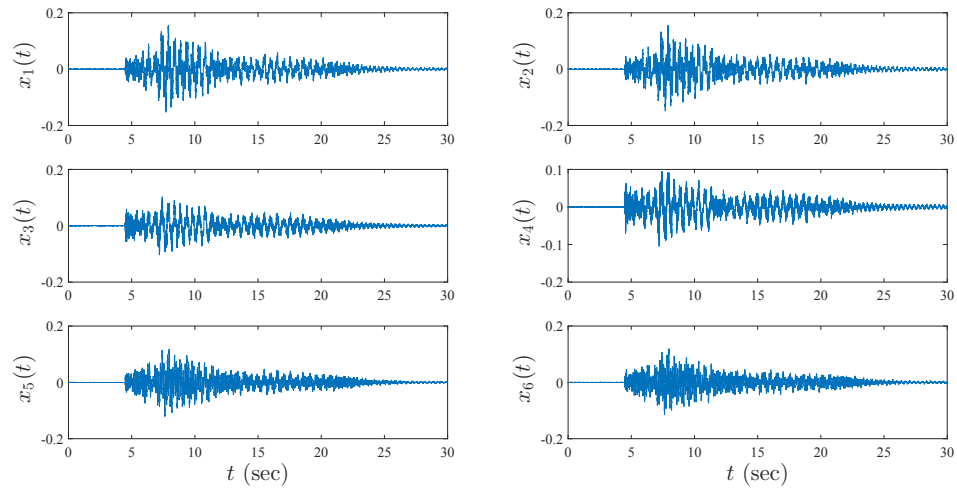


Figure 5.14: Time history of floor responses obtained from Model B before damage (ground motions)

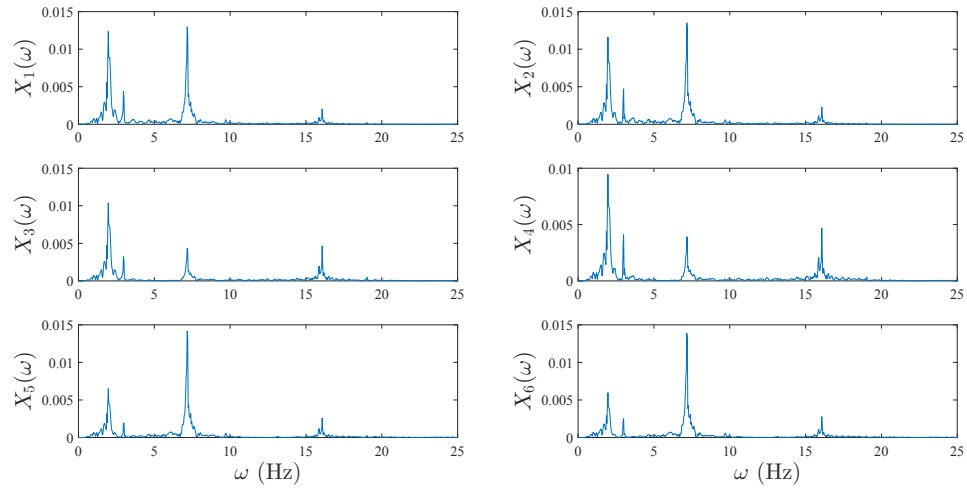


Figure 5.15: Fourier spectrum of floor responses obtained from Model B before damage (ground motions)

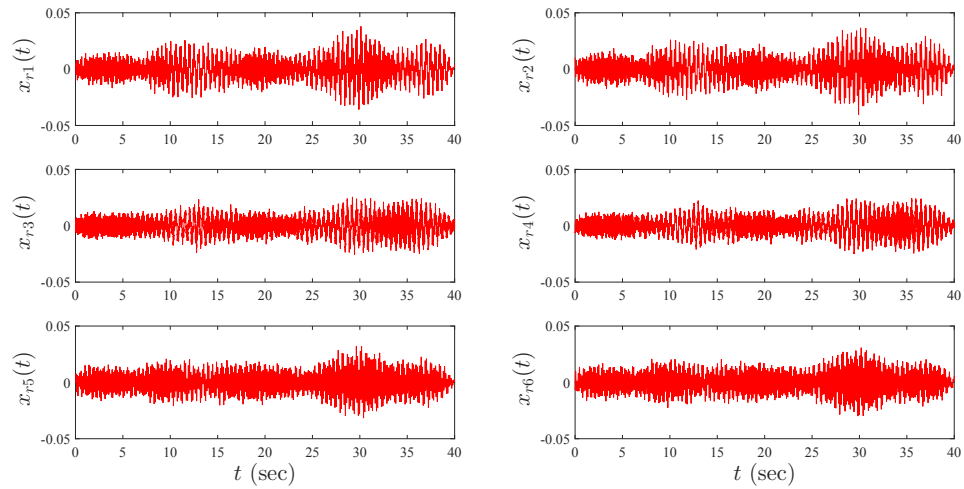


Figure 5.16: Time history of floor responses obtained from the reconstructed data by DCT (white noise)

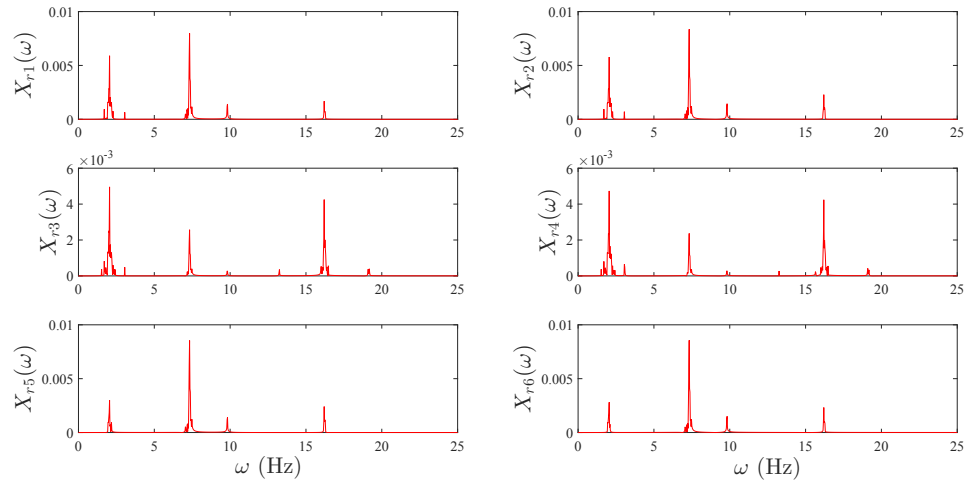


Figure 5.17: Fourier spectrum of floor responses obtained from the reconstructed data by DCT (white noise)

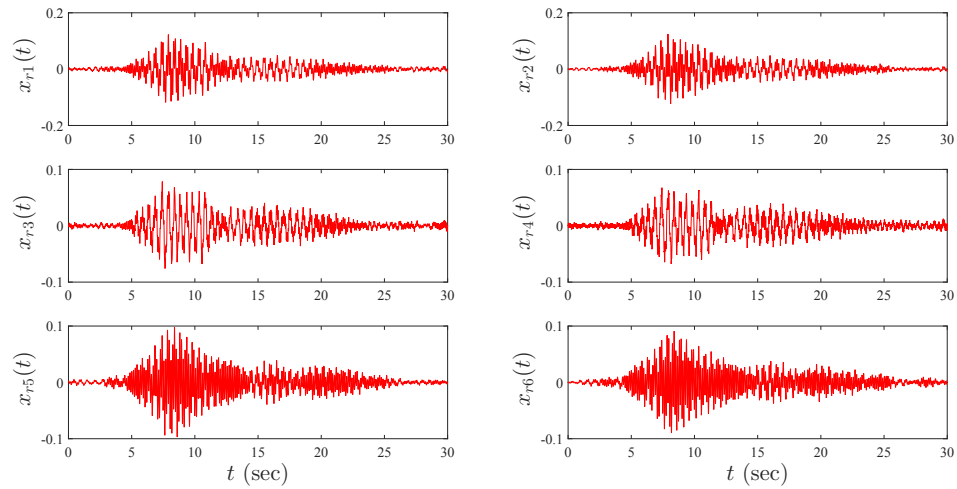


Figure 5.18: Time history of floor responses obtained from the reconstructed data by DCT (ground motions)

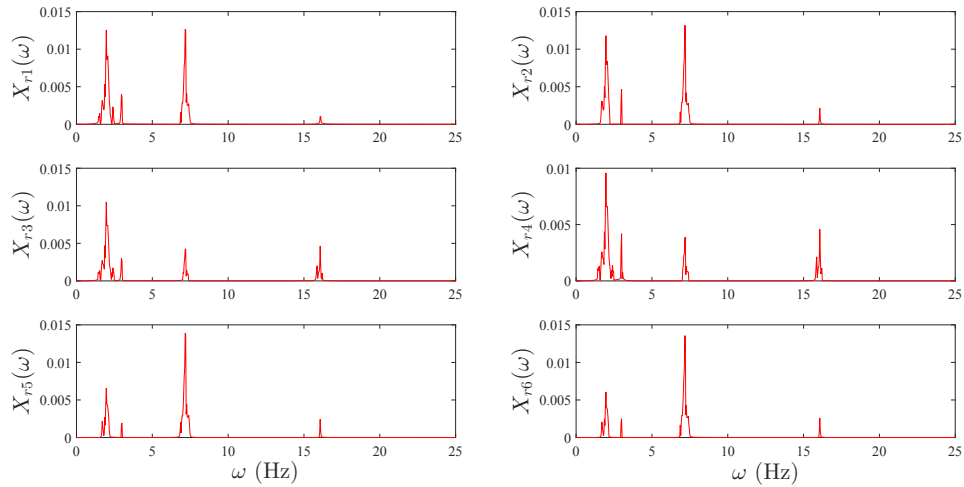


Figure 5.19: Fourier spectrum of floor responses obtained from the reconstructed data by DCT (ground motions)

As a result, the six signals of floor responses observed from the model with subjected to white noise illustrate the resulting natural frequencies of each signal which are 2, 7.3 and 16.2 Hz, as indicated in Fig. 5.13, whereas the index of natural frequencies extracted from the time history of each signal of the ground motion test are 2, 7.2 and 16.1 Hz, as shown in Fig. 5.15. The performance of the proposed method is presented using the observed data from white noise and ground motion testing. This compression method is applied with a threshold rate of 12% of the maximum DCT energy considered in each signal in order to discard samples below the threshold level. This process minimizes the size of the data norm to achieve compression and then recover the compressed signal through IDCT. Compared to the original data observed from both tests, it is clear that the reconstructed signals through DCT data compression have maintained the significant characteristics of the signals, where data recovery seems satisfactory since the reconstructed Fourier spectra in Fig. 5.17 and Fig. 5.19 show similar modal frequencies with a slight difference of amplitude. With these results, it is clear that DCT is able to reflect correct dynamic behaviour of the

structure in the reconstructed data under both random and ground motion data.

In order to check the efficiency of data compression through DCT, application of TFBSS is performed to separate the modal frequencies observed from the white noise test. The objective of TFBSS application is to separate multi-component signals and represent them as sources of the collected signals where each source produces a single natural frequency. Therefore, this separation can be exploited to check robustness of data compression using DCT. A data set of 3 seconds is taken from the time histories (i.e., from 25 to 28 seconds) of the white noise test shown in Fig. 5.12. Date compression using DCT is applied with a threshold level of 12% of the maximum DCT energy to neglect values below the limit, and then IDCT is performed to reconstruct the signals. Application of TFBSS is performed on the original and reconstructed signals to extract modal responses whose Fourier spectra are shown in Fig. 5.20. Results of TFBSS prove that data compression through DCT is reliable and satisfactory due to accomplishment of compression with accurate data recovery as the reconstructed data seems very similar to the results of the original data.

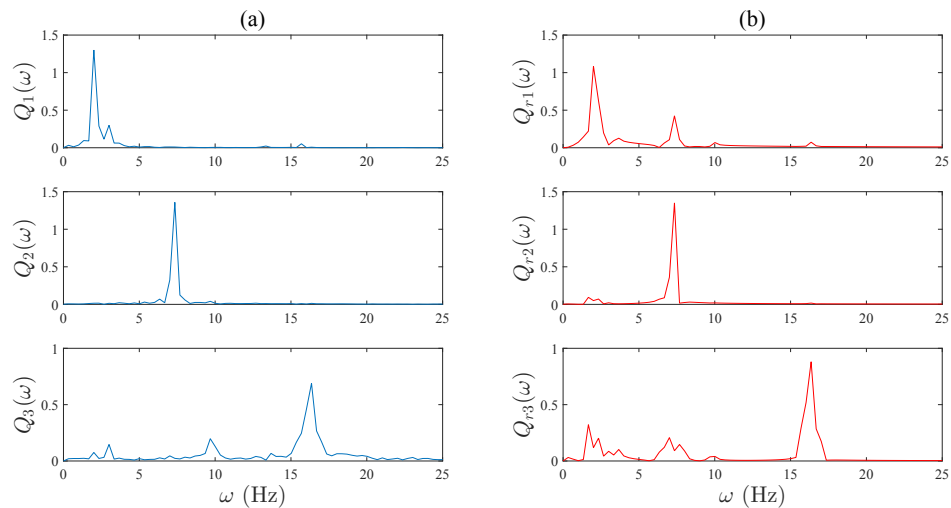


Figure 5.20: Fourier spectra of modal responses using TFBSS obtained from (a) original data and (b) reconstructed data by DCT

5.2.2 Effect of Discrete Damage

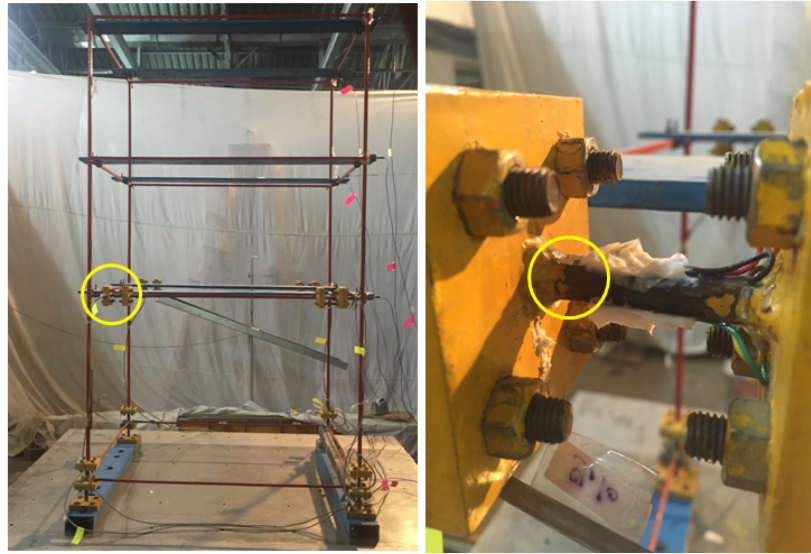


Figure 5.21: Damage occurs on first level of Model B due to loosening of bolt

In the previous model, damage is artificially initiated near the end of one beam of the first level, as indicated in Fig. 5.21. In this way, the performance of DCT could be checked to reconstruct data with damage-induced signature as compared to baseline model. For white noise test, the time histories and Fourier spectra of floor responses obtained from each accelerometer located on the model are respectively illustrated in Fig. 5.22 and Fig. 5.23, while the time histories and Fourier spectra of floor responses obtained from the ground motion test are respectively shown in Fig. 5.24 and Fig. 5.25. Data compression through DCT is then performed on the data observed from the white noise test, as shown in Fig. 5.26 and Fig. 5.27, whereas the reconstructed time histories and their Fourier spectra of floor responses obtained from the ground motion test are respectively indicated in Fig. 5.28 and Fig. 5.29.

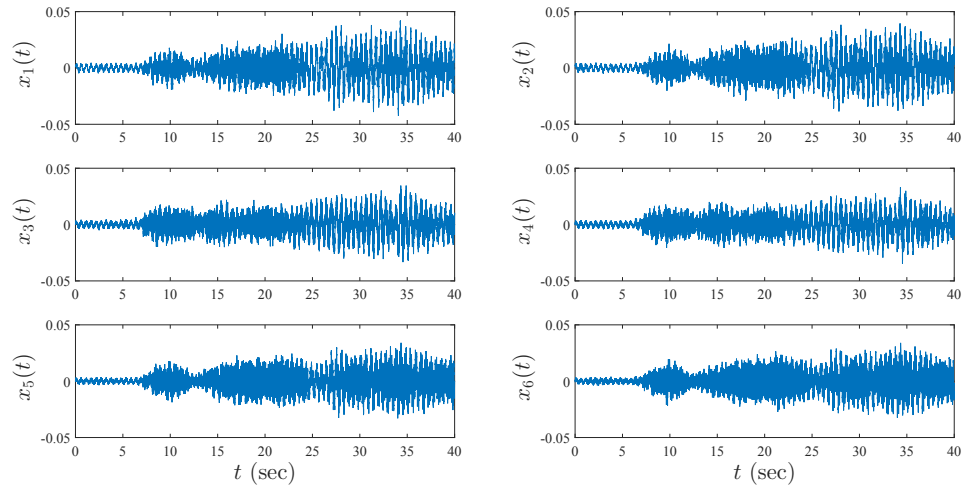


Figure 5.22: Time history of floor responses obtained from Model B after damage (white noise)

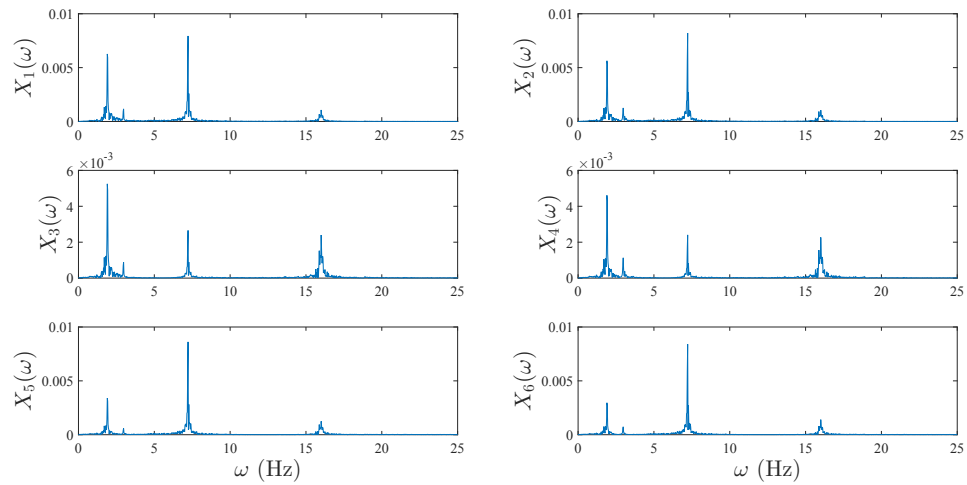


Figure 5.23: Fourier spectrum of floor responses obtained from Model B after damage (white noise)

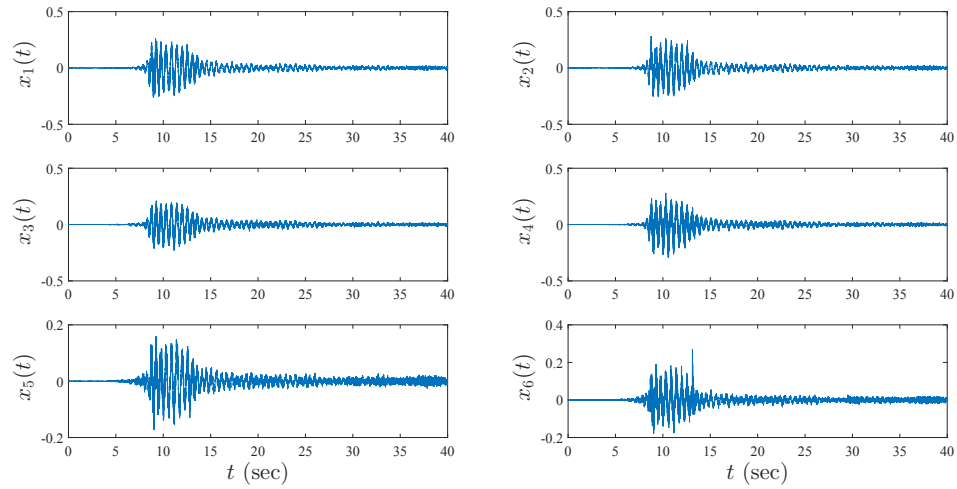


Figure 5.24: Time history of floor responses obtained from Model B after damage (ground motions)

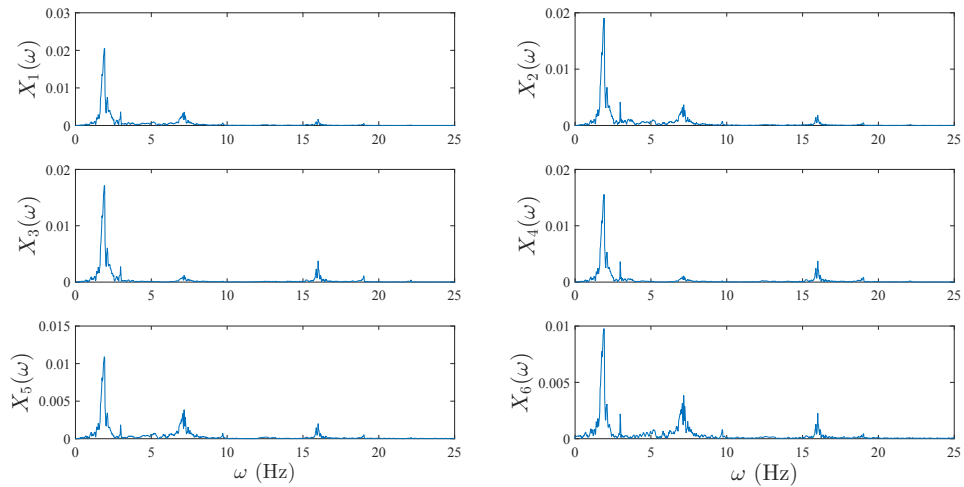


Figure 5.25: Fourier spectrum of floor responses obtained from Model B after damage (ground motions)

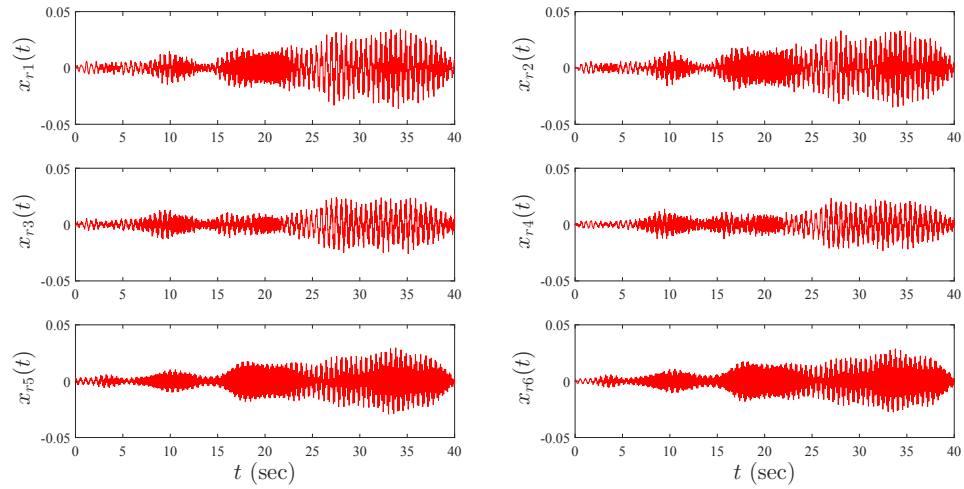


Figure 5.26: Time history of floor responses obtained from the reconstructed data by DCT (white noise)

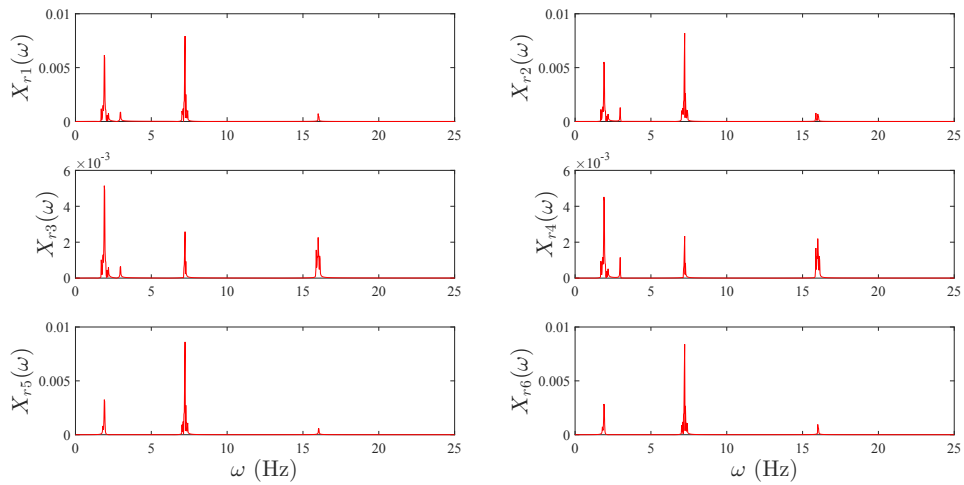


Figure 5.27: Fourier spectrum of floor responses obtained from the reconstructed data by DCT (white noise)

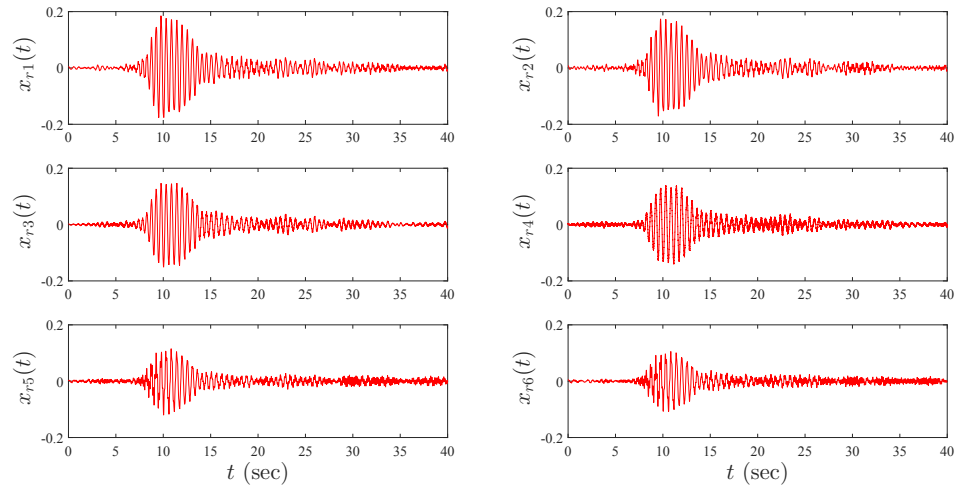


Figure 5.28: Time history of floor responses obtained from the reconstructed data by DCT (ground motions)

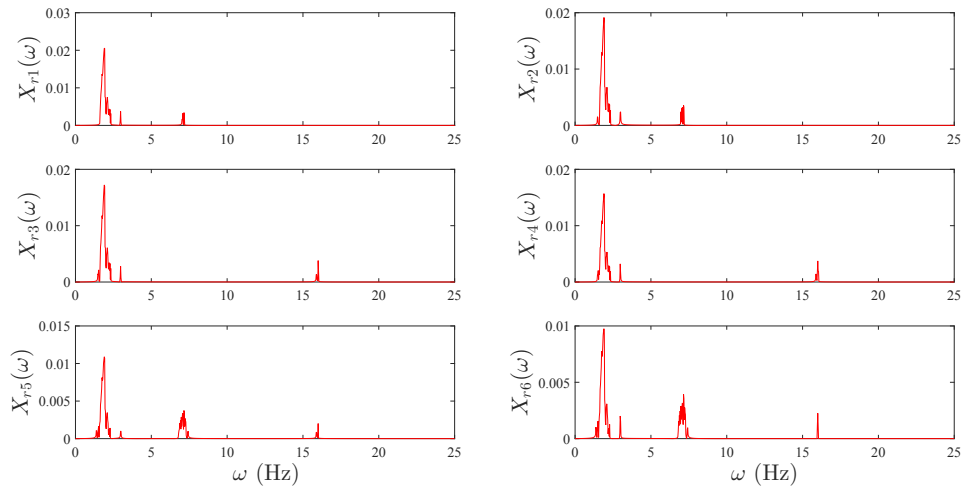


Figure 5.29: Fourier spectrum of floor responses obtained from the reconstructed data by DCT (ground motions)

As a result, the six signals of floor responses observed from the model with subjected white noise illustrate the index of natural frequencies extracted from the time history of each signal which are 1.9, 7.2 and 16 Hz, as indicated in Fig. 5.23, whereas the index of natural frequencies extracted from the time history of each signal of the ground motion test are 1.9, 7.2 and 16 Hz, as shown in Fig. 5.25. The performance

of the proposed method is presented using the observed data from both tests. DCT is applied with a threshold rate of 12% of the maximum DCT energy considered in each signal to discard samples below the threshold level. This process minimizes the size of the data norm to achieve compression and then recover the compressed signal through IDCT. Compared to the original data observed from both tests, it is clear that the reconstructed signals through DCT data compression have maintained the significant characteristics of the signals, where data recovery seems satisfactory since the reconstructed Fourier spectra in Fig. 5.27 and Fig. 5.29 show the exact values of actual natural frequencies with a slight difference of amplitude.

In order to check the efficiency of data compression through DCT, application of TFBSS is performed to separate the natural frequencies observed from the white noise test. To perform this application, a sample data of 3 seconds is taken from the time histories (i.e., from 25 to 28 seconds) of the white noise test shown in Fig. 5.22, and their Fourier spectra are generated. Data compression using DCT is applied with a threshold level of 12% of the maximum DCT energy to neglect values below the limit, and then IDCT is performed to reconstruct the signals. Application of TFBSS is performed on the original and reconstructed signals to extract modal responses and represent the natural frequencies separately in Fig. 5.30 where the outputs of the reconstructed data show almost the exact values as the results of the original data. Summary of frequency analysis obtained from the original and reconstructed data by DCT is indicated in Table 5.2 for damaged and undamaged tests. Results of TFBSS prove that data compression through DCT is a robust technique that can recover the signals from fewer measurements.

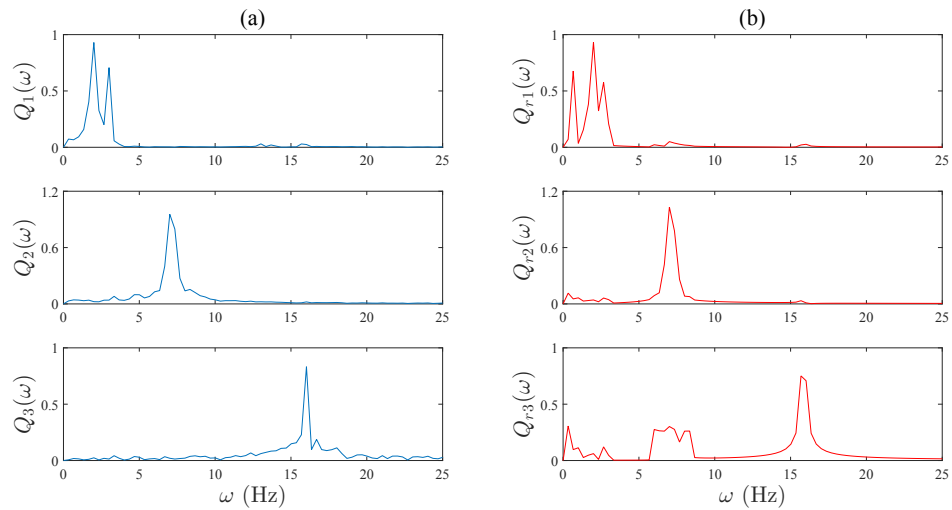


Figure 5.30: Fourier spectra of modal responses using TFBSS obtained from (a) original data and (b) reconstructed data by DCT

Table 5.2: Summary of TFBSS results obtained from the original and reconstructed data by DCT for undamaged and damaged tests

Type of test	Baseline						With Damage					
	$X(\omega)$			$X_r(\omega)$			$X(\omega)$			$X_r(\omega)$		
ω_i (Hz)	ω_1	ω_2	ω_3	ω_1	ω_2	ω_3	ω_1	ω_2	ω_3	ω_1	ω_2	ω_3
White noise	2	7.3	16.3	2	7.3	16.3	1.9	7.2	16	1.9	7.2	16
Ground motion	2	7.2	16.1	2	7.2	16.1	1.9	7.2	16	1.9	7.2	16

5.3 Cantilever Beam

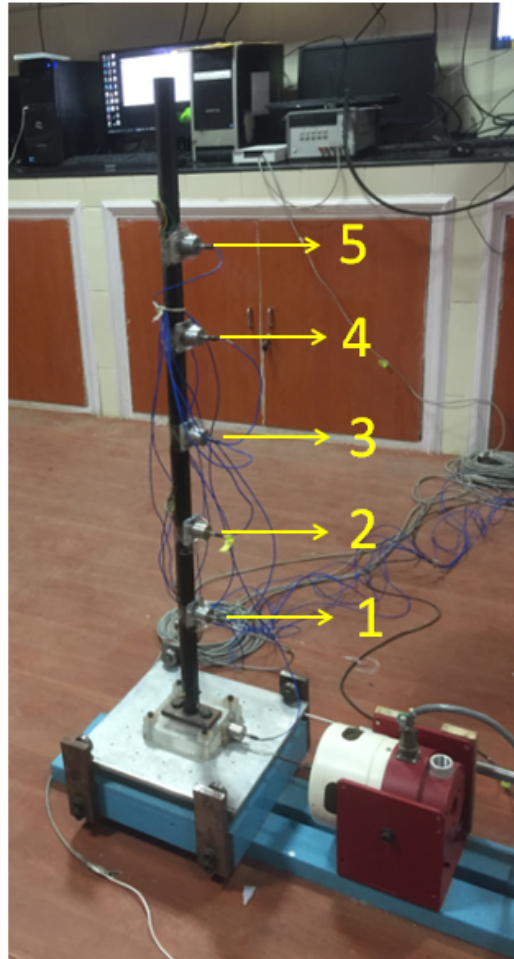


Figure 5.31: Cantilever beam attached with a shaker and accelerometers at IIT Kanpur

A 1 m long hexagonal cantilever beam is utilized to perform necessary data processing in order to determine its natural frequency and exploit the data compression techniques. The testing is performed using wired sensors set with sampling frequency of 1000 Hz under random base excitation. Five wired sensors are installed on the beam as illustrated in Fig. 5.31 where the signals correspond to the sequence of sensors. Plots of the time histories and Fourier spectra are generated to present the natural

frequency of this cantilever beam as shown respectively in Fig. 5.32 and 5.33. In addition, data compression using DCT is performed on the collected data and presented in Fig. 5.34 and Fig. 5.35.

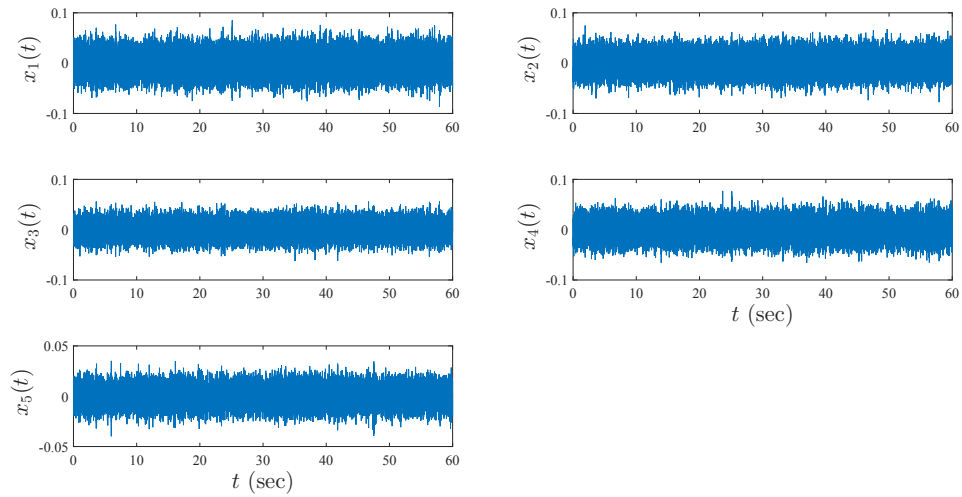


Figure 5.32: Time history of the beam responses under random base excitation

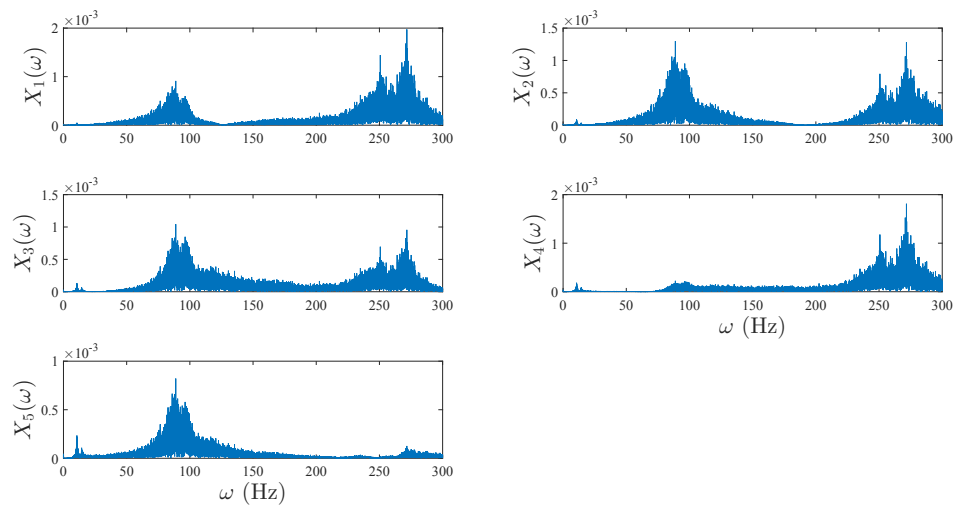


Figure 5.33: Fourier spectrum of the beam responses under random base excitation

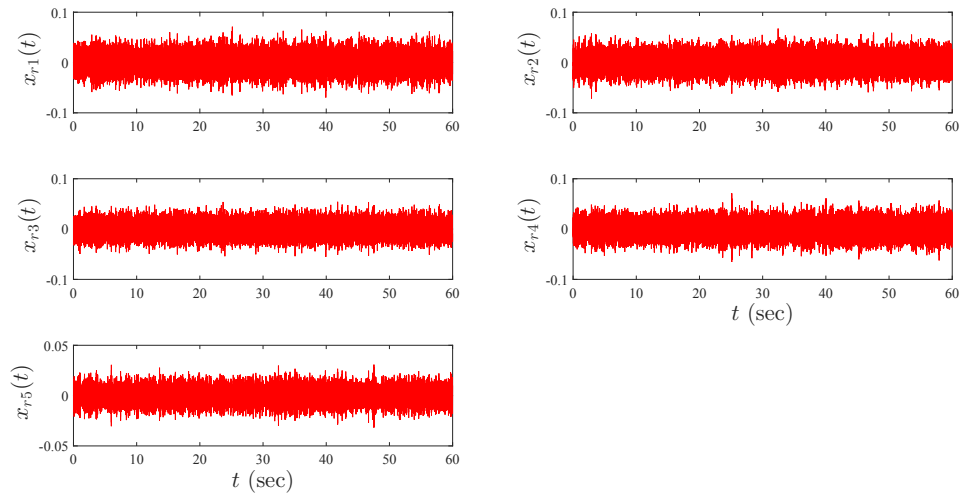


Figure 5.34: Time history of the beam responses obtained from the reconstructed data

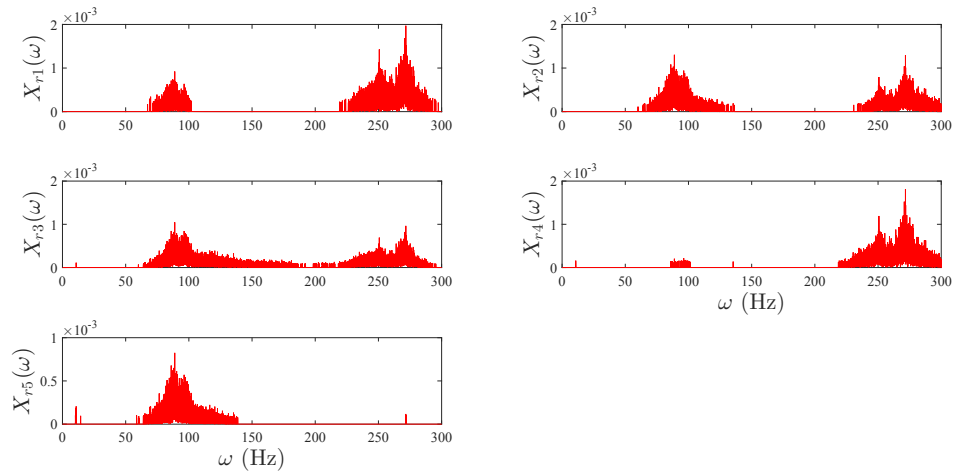


Figure 5.35: Fourier spectrum of the beam responses obtained from the reconstructed data

As a result, the five signals of the beam responses observed from the model with subjected random force illustrate the index of natural frequencies extracted from the time history of each signal which are 10, 88, and 270 Hz, as indicated in Fig. 5.33. The performance of the proposed method is presented using the observed data where

data compression is applied with a threshold rate of 10% of the maximum DCT energy considered in each signal in order to neglect values below the threshold level. This process minimizes the size of the data norm to achieve compression and then recover the compressed signal through IDCT. Compared to the original data, it is clear that the reconstructed signals through DCT data compression have maintained the significant characteristics of the signals, where data recovery seems satisfactory since the reconstructed Fourier spectra in Fig. 5.34 and Fig. 5.35 show the exact values of actual natural frequencies.

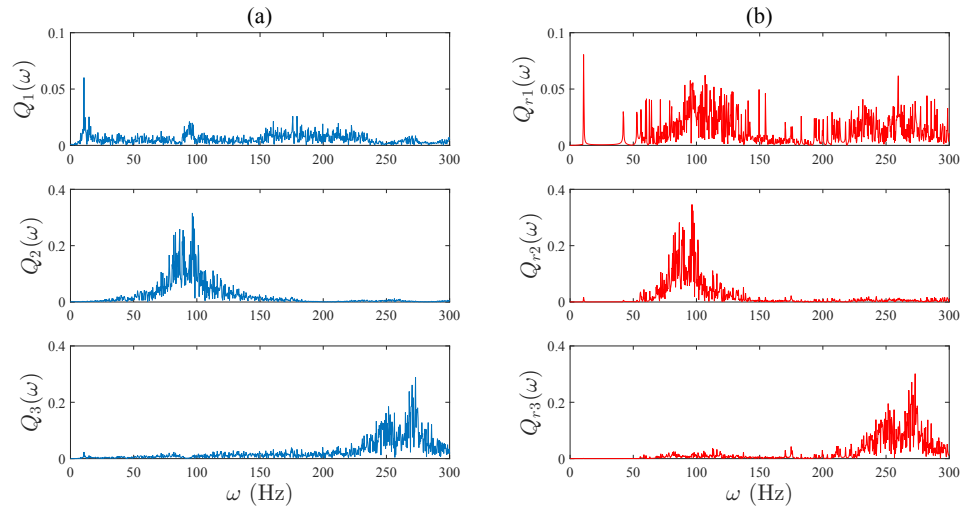


Figure 5.36: Fourier spectra of modal responses using TFBSS obtained from (a) original data and (b) reconstructed data by DCT

In order to check the efficiency of data compression through DCT, application of TFBSS is performed to separate the observed natural frequencies. To perform this application, a sample data of 10 seconds is taken from the time histories as shown in Fig. 5.32 (i.e., from 15 to 18 seconds), and their Fourier spectra are generated. After data compression by DCT is performed on these signals, TFBSS is then applied to present the modal responses extracted from the original and reconstructed data in Fig. 5.36 where the original and reconstructed Fourier spectrum present the exact

values of 10, 95 and 270 Hz. Results of TFBSS prove that data compression through DCT is reliable and satisfactory as data compression is achieved with accurate data recovery.

5.4 Full-scale Study



Figure 5.37: Long-span bridge in Thunder Bay

The Main Street Bridge as shown in Fig. 5.37 is located in Thunder Bay, Canada. It was built in 1960, its length and width are 288 m and 9 m, respectively. The bridge is supported by 11 piers and maximum height of these piers is 8 m and the spacing between piers is 53 m. In order to conduct the serviceability assessment of this bridge, vibration testing was performed on January 20th, 2017 between 9 am - 12 noon. The temperature during the test was approximately -5°C . Six sensors were placed along the walkway on the North side of the bridge. Sensors were set up to measure uniaxial vibration in the vertical direction. The data acquisition (DAQ) system is placed at the centerline of the bridge and the spacing of the sensors were roughly 10, 100 and 200 feet off either side of the DAQ. Tests were conducted with various numbers of vehicles crossing the bridge at different speeds (50-60 km/h).

Collected data of one wired sensor from one test is utilized to validate the proposed methods, LNM and DCT. This data is used to apply compression in order to check accuracy of reconstruction with considering several rates of compression. Sampling frequency is here set to be 200 Hz, and only 5000 samples are used for processing. Using different rates of compression indicates how reconstruction can be effective using the LNM and DCT methods.

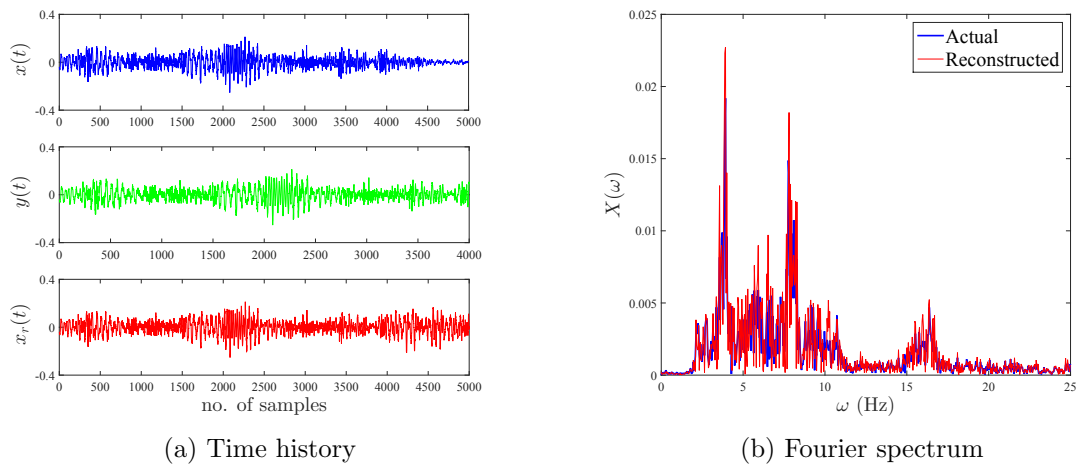


Figure 5.38: 20% data compression by LNM

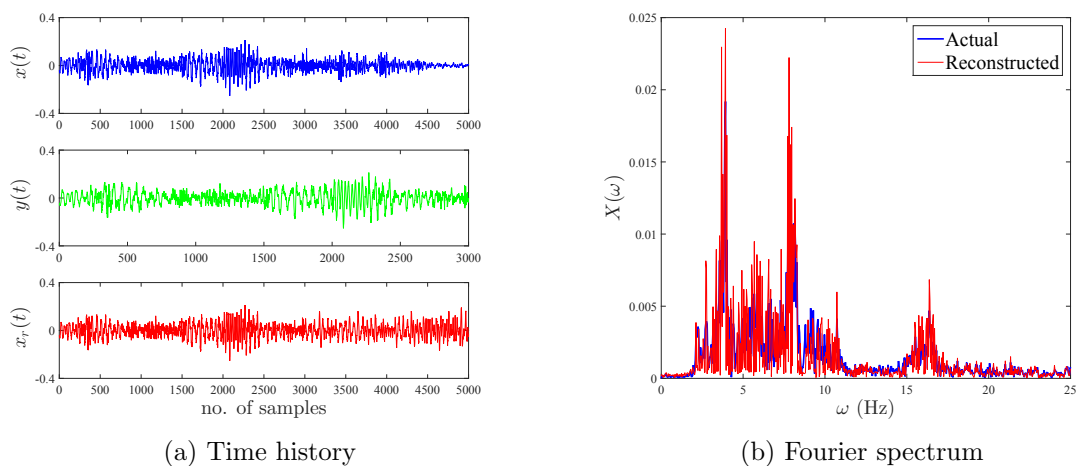


Figure 5.39: 40% data compression by LNM

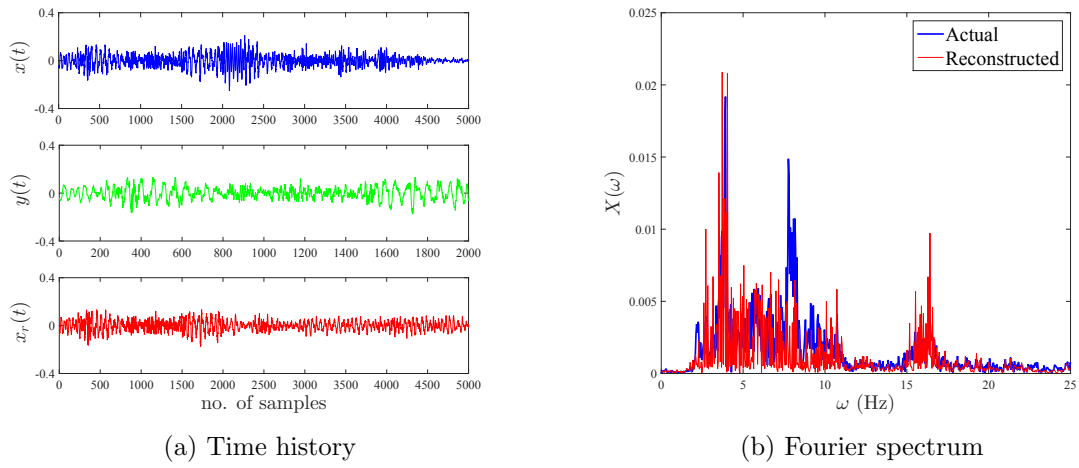


Figure 5.40: 60% data compression by LNM

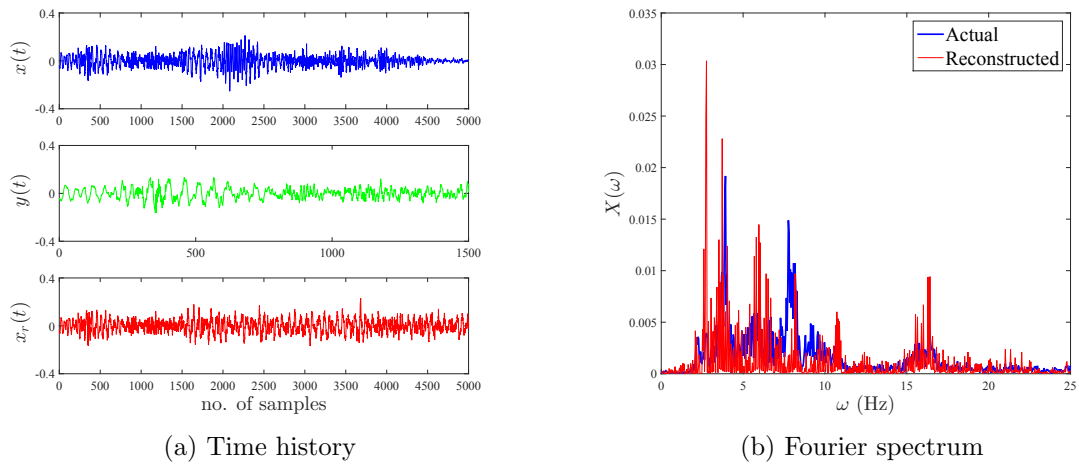


Figure 5.41: 70% data compression by LNM

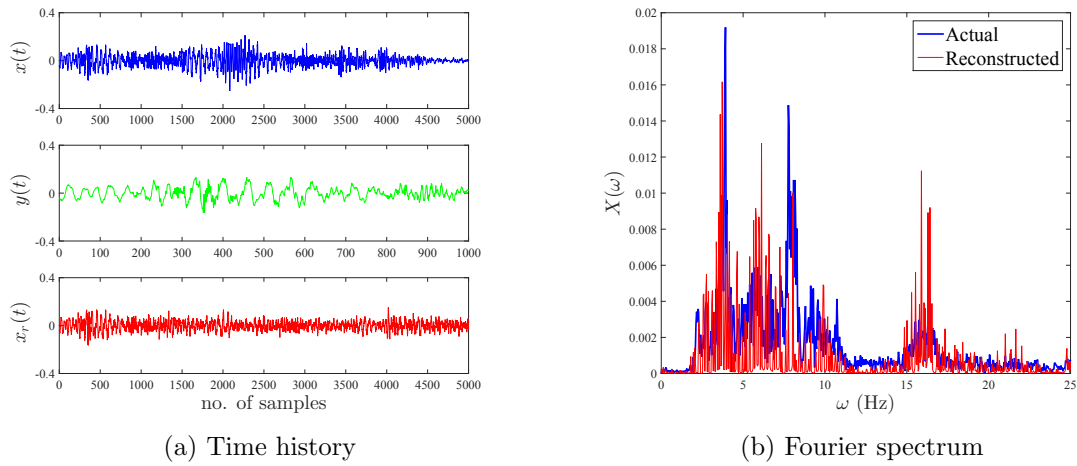


Figure 5.42: 80% data compression by LNM

The selected rates of 20%, 40%, 60%, 70% and 80% are indicated above respectively in Fig. 5.38, Fig. 5.39, Fig. 5.40, Fig. 5.41 and Fig. 5.42; where $x(t)$ is original, $y(t)$ is compressed and $x_r(t)$ is reconstructed. Reconstructed Fourier spectrum is almost same as the actual outputs which indicates a sign of a reliable recovery technique. High rates of data compression clearly results inaccurate reconstruction especially when exceeding the rate of 40%, as illustrated in the above plots, because measurements of under-sampled signals are insufficient to recover the signals. It is meant to exceed the minimum percentage of compression, set by the Shannon theory, in order to distinguish the efficiency of different compression rates.

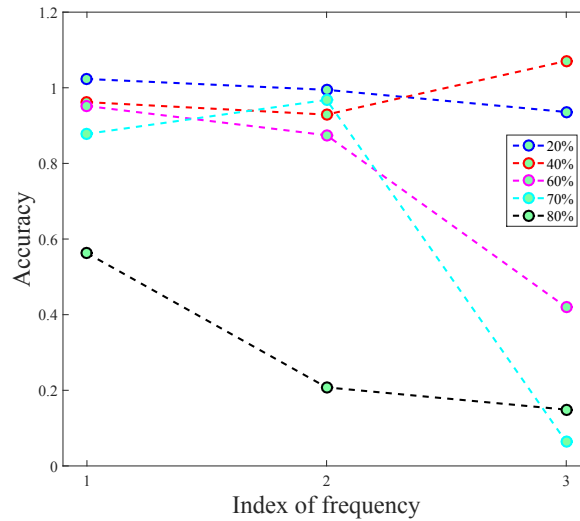


Figure 5.43: Accuracy of data reconstruction for all selected rates of compression

Index of frequency is summarized in Fig. 5.43 to present the accuracy of identifying modal frequencies as obtained in the Fourier spectra. Except 80% compression, the compression rate shows better performance under 20% and 40% compression. In case of 60% and 70% compression, the accuracy of third modal frequency is compromised. As such, it is clear that CS is a promising technique that can efficiently recover signals from fewer measurements. CS through LNM has proven its workability of reconstructing sparse signals and potentially avoids the issue of missing data while transmitting. However, accuracy of data reconstruction has become another challenge encountering this method. As shown in Fig. 5.43, high rates of compression result useless reconstruction whereas compressing a low rate of samples ensures perfect recovery of the compressed signal.

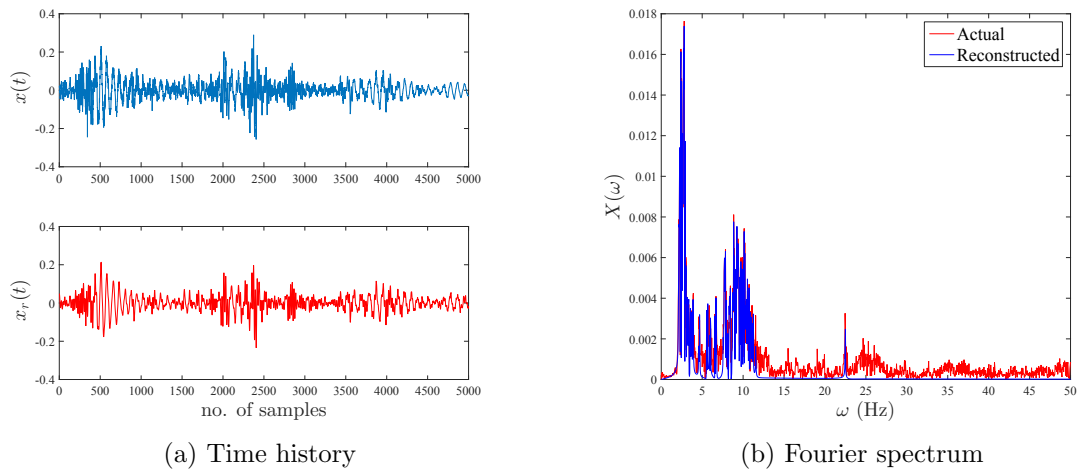


Figure 5.44: Compression by DCT with 10% threshold level

The performance of the proposed DCT method is presented using observed data from the bridge in Fig. 5.44 and the signals are then reconstructed through IDCT. As shown in Fig. 5.45, the Fourier spectra of modal responses using TFBSS are generated to test the reconstructed data by LNM and DCT, where the values of natural frequencies are indicated in Table 5.3. The reconstructed data by DCT has produced the same values of modal responses with some mode mixing but at least the reconstructed Fourier spectra seem very similar to the original outputs. However, the reconstructed data by LNM generates the Fourier spectra of model responses with significant mode mixing. Results prove that the performance of DCT method is better than the performance of LNM in data compression even for a real-life structure.

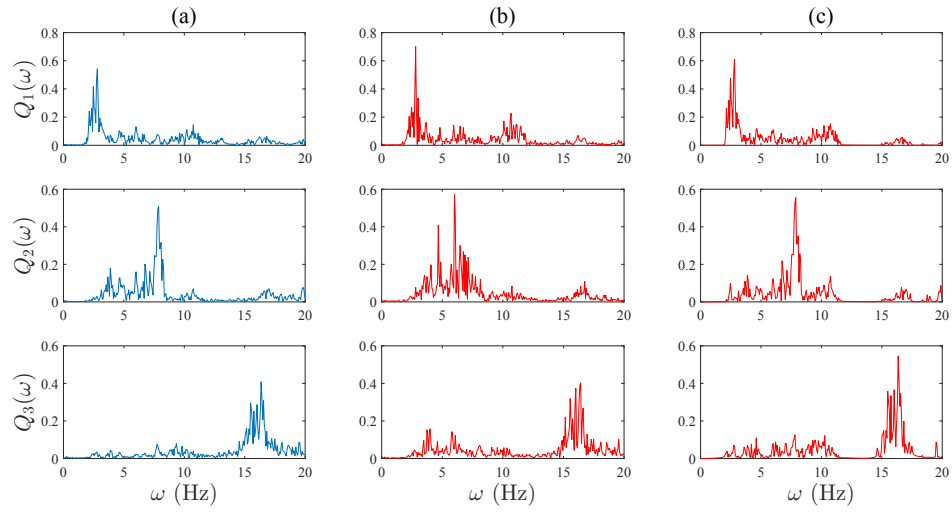


Figure 5.45: Fourier spectra of modal responses using TFBS obtained from (a) original data, (b) reconstructed data by LNM and (c) reconstructed data by DCT

Table 5.3: Identification results using the original and reconstructed data by LNM and DCT

ω_i (Hz)	ω_1	ω_2	ω_3
Actual	2.8	7.88	16.36
LNM	2.8	6.01	16.42
DCT	2.8	7.88	16.36

Chapter 6

Conclusions and Future Work

Detailed conclusions of the thesis are provided in this chapter to summarize the outcome of the proposed research towards solving the big data issue in structural health monitoring. Finally, several recommendations are made to contribute further in this area as future research.

6.1 Key Conclusions

- DCT is exploited as a data compression technique that can deal with big data measured from the structural systems. The performance of DCT is compared with the LNM under a wide range of simulation and experimental models.
- The results show improved performances of DCT with respect to LNM under various data compression rates, even up to 60%.
- Apart from comparing merely time-structure of data, a newer system identification algorithm (i.e., TFBSS), is adopted to perform modal identification and evaluate the performance of DCT in identifying accurate modal frequencies from the reconstructed data. With this unique approach, the accuracy of data reconstruction is verified not only using the time-domain, but also in frequency domain.
- Simulation results show that the DCT-assisted reconstructed data results in

successful identification of all target modes of a 10-DOF model. On the other hand, LNM yields significant mode-mixing in the resulting modal responses.

- Both implicit and explicit data compression are performed using wireless sensors where DCT shows better performance compared to LNM. Wireless sensor-based implicit data compression proves the capability of DCT's data reconstruction in real-time application.
- With the aid of a realistic experimental model, it is shown how DCT is able to reconstruct data with damage signatures. The TFBSS are then applied and the results show the identified frequencies accurately represent both undamaged and damaged structures.
- Even with low energy modes and measurement noise, the DCT-assisted data compression has been successful in identifying modal frequencies of a long-span bridge.

6.2 Achievements

- Received Mitacs Gloablink Research Award to conduct relevant research internship in IIT Kanpur, India.

6.3 Future Work

In this thesis, the proposed research is aimed to handle big data collected from structural systems. The results show the improved performance of DCT in data reconstruction containing a wide range of dynamical characteristics including low energy

modes, measurement noise and damage signatures. Further recommendations are made to contribute in this area.

- Embed the data compression algorithms within the sensor boards such that real-time data compression can be achieved during the long-term monitoring of structure and reduce the amount of big data further. This research will be employed by collaborating with researchers in Computer Science and Electrical Engineering departments.
- As data compression through DCT is used with a threshold function, the effect of signal-to-noise ratio will be considered to automate setting up the threshold level.
- In case of missing data, the performance of data compression needs to be investigated. Several numerical studies and experimental research are required to be pursued to initiate this study.
- More implicit data compression is recommended to be performed for full-scale structures using wireless sensors.

6.4 Acronyms

Following is the list of all relevant acronyms used in this thesis for the convenience of the readers.

Table 6.1: List of acronyms

SHM	Structural health monitoring
WSN	Wireless sensor network
CS	Compressive sensing
LNM	L_1 -norm minimization
DCT	Discrete cosine transform
DFT	Discrete Fourier transform
IDCT	Inverse discrete cosine transform
TFBSS	Time-frequency blind source separation
DAQ	Data acquisition
DOF	Degree-of-freedom
BCS	Bayesian compressive sensing
BSS	Blind source separation
MSE	Mean square error
CR	Compression ratio

Bibliography

- [1] Carden, P. and Fanning, P. (2004). "Vibration Based Condition Monitoring: A Review." *Structural Health Monitoring*, 3(4): 355-377.
- [2] Li, X., Yu, W. and Villegas, S. (2016). "Structural Health Monitoring of Building Structures With Online Data Mining Methods." *IEEE Systems Journal*, 10(3): 1291-1300.
- [3] Duan, Z. and Zhang, K. (2006). "Data Mining Technology for Structural Health Monitoring." *Pacific Science Review*, 8: 27-36.
- [4] Fraser, M., Elgamal, A., He, X. and Conte, J. (2010). "Sensor Network for Structural Health Monitoring of a Highway Bridge." *Journal of Computing in Civil Engineering*, 24(1): 11-24.
- [5] Lynch, J. and Loh, K. (2006). "A Summary Review of Wireless Sensors and Sensor Networks for Structural Health Monitoring." *The Shock and Vibration Digest*, 38(2): 91-128.
- [6] Lynch, J., Sundararajan, A., Law, K., Kiremidjian, A. and Carryer, E. (2003). "Power-efficient Data Management for a Wireless Structural Monitoring System." *Proceedings of the 4th International Workshop on Structural Health Monitoring, Stanford, Stanford, CA, USA*.
- [7] Hohrath, B. (2013). "A Comparison of NARADA and IMOTE2 WSU for Structural Health Monitoring of Bridges."
- [8] Lima, M., Sales, C., Santos, A., Santos, R., Silva, M., Costa, J., Carvalho, M. and Cruz, M. (2016). "A Framework for Data Compression and Damage Detection in Structural Health Monitoring Applied on a Laboratory Three-story Structure." *Revista Brasileira de Computao Aplicada*, 8(2): 129-143.
- [9] Park, S., Lee, J., Yun, C. and Inman, D. "PCA-Data Compression for Impedance-Based Wireless Structural Health Monitoring Framework."
- [10] Cai, G. and Mahadevan, S. (2016). "Big Data Analytics in Online Structural Health Monitoring." *International Journal of Prognostics and Health Management*, 2153-2648.
- [11] Candes, E. and Wakin, M. (2008). "An Introduction to Compressive Sampling." *IEEE Signal processing magazine*, 25(2): 21-30.

- [12] Bao, Y., Beck, J. and Li, H. (2011). “Compressive Sampling for Accelerometer Signals in Structural Health Monitoring.” *Structural Health Monitoring*, 10(3): 235-246.
- [13] Li, S., Yang, D., Tang, G. and Wakin, M. (2017). “Atomic Norm Minimization for Modal Analysis from Random and Compressed Samples.”
- [14] Jayawardhana, M., Zhu, X., Liyanapathirana, R. and Gunawardana, U. (2017). “Compressive Sensing for Efficient Health Monitoring and Effective Damage Detection of Structures.” *Mechanical Systems and Signal Processing*, 84: 414-430.
- [15] Ganesan, V., Das, T., Rahnavard, N. and Kauffman, J. (2017). “Vibration-based Monitoring and Diagnostics Using Compressive Sensing.” *Journal of Sound and Vibration*, 394: 612-630.
- [16] Huang, Y., Beck, J., Wu, S. and Li, H. (2016). “Bayesian Compressive Sensing for Approximately Sparse Signals and Application to Structural Health Monitoring Signals for Data Loss Recovery.” *Probabilistic Engineering Mechanics*, 46: 62-79.
- [17] Bao, Y., Wang, X., Shi, Z. and Li, H. (2016). “Group Sparse Optimization Based-compressive Sensing of Vibration Data Using Wireless Sensors for Structural Health Monitoring.”
- [18] Sadhu, A., Hu, B. and Narasimhan, S. (2012). “Blind Source Separation Towards Decentralized Model Identification Using Compressive Sampling.” *The 11th International Conference on Information Sciences*.
- [19] Ji, S., Huang, L., Wang, J., Shen, J. and Kim, J. (2014). “An Improved Reconstruction Method of Compressive Sensing Data Recovery in Wireless Sensor Networks.” *International Journal of Security and Its Applications*, 8(1): 1-8.
- [20] Gkoktsi, K. and Giaralis, A. (2017). “Assessment of Sub-Nyquist Deterministic and Random Data Sampling Techniques for Operational Modal Analysis.” *Structural Health Monitoring*, 16(5): 630-646.
- [21] Yang, Y. and Nagarajaiah, S. (2017). “Robust Data Transmission and Recovery of Images by Compressed Sensing for Structural Health Diagnosis.” *Structural Control and Health Monitoring*, 24(1): 18-56.
- [22] Nagarajaiah, S. and Yang, Y. (2017). “Modeling and Harnessing Sparse and Low-rank Data Structure: A New Paradigm for Structural Dynamics, Identification, Damage Detection, and Health Monitoring.” *Structural Control and Health Monitoring*, 24(1): 18-51.
- [23] Delsys. (2010). “Trigno Wireless System.” Retrieved from www.delsys.com
- [24] Le, T. and Paultre, P. (2012). “Modal Identification Based on Continuous Wavelet Transform and Ambient Excitation Tests.” *Journal of Sound and Vibration*, 331(9): 2023-2037.

- [25] Yang, A., Ganesh, A., Zhou Z., Sastry, S. and MA, Y. (2010). "A Review of Fast L_1 -minimization Algorithms for Robust Face Recognition."
- [26] Donoho, D. (2006). "Compressed Sensing." *IEEE Transactions on Information Theory*, 52(4): 1289-1306.
- [27] Nahar, P., and Kolte, M. (2014). "An Introduction to Compressive Sensing and its Applications." *International Journal of Scientific and Research Publications*. 4(6), 2250-3153.
- [28] Zou, Z., Bao, Y., Li, H., Spencer, B. and Ou, J. (2015). "Embedding Compressive Sensing-Based Data Loss Recovery Algorithm Into Wireless Smart Sensors for Structural Health Monitoring." *IEEE Sensors Journal*, 15(2): 797-808.
- [29] Zou, Z., Bao, Y., Deng, F. and Li, H. (2015). "An Approach of Reliable Data Transmission With Random Redundancy for Wireless Sensors in Structural Health Monitoring." *IEEE Sensors Journal*, 15(2): 809-818.
- [30] Raid A., Khedr, W., El-dosuky, M. and Ahmed, W. (2014). "Jpeg Image Compression Using Discrete Cosine Transform - A Survey." *International Journal of Computer Science and Engineering Survey*, 5(2).
- [31] Bagul, S., Shimpi, N. and Patil, P. (2014). "JPEG Image Compression Using Fast 2-D DCT Technique." *International Journal of Advanced Research in Computer and Communication Engineering*, 3(11), 2278-1021.
- [32] Zhou X., Bai, Y. and Wang, C. (2015). "Image Compression Based on Discrete Cosine Transform and Multistage Vector Quantization" *International Journal of Multimedia and Ubiquitous Engineering*, 10(6): 347-356.
- [33] Fracastoro, G., Fosson, S. and Magli, E. (2017). "Steerable Discrete Cosine Transform" *IEEE Transactions on Image Processing*, 26(1): 303-314.
- [34] Ahmed, N., Natarajan, T. and Rao, K. (1974). "Discrete cosine transform." *IEEE Transactions on Computers*, 23(1): 90-93.
- [35] Kitajima, J. (1980). "A Symmetric Cosine Transform." *IEEE Transactions on Computers*, C-29(4): 317-323.
- [36] Sadhu, A., Narasimhan S. and Antoni, J. (2017). "A Review of Output-only Structural Mode Identification Literature Employing Blind Source Separation Methods." *Mechanical Systems and Signal Processing*, 94: 415-431.
- [37] Fvotte, C. and Doncarli, C. (2004). "Two Contributions to Blind Source Separation Using Time-Frequency Distributions." *IEEE Signal Processing Letters*, 11(3): 386-389.

- [38] Musafere, F., Sadhu, A. and Liu, K. (2015). “Towards Damage Detection Using Blind Source Separation Integrated with Time-varying Auto-regressive Modeling.” *Smart Materials and Structures*, 25(1), 015013.
- [39] Pal, S., Datta, A. and Pal, N. R. (2001). “A Multilayer Self-organizing Model for Convex-hull Computation.” *IEEE Transactions on Neural Networks*, 12(6): 1341-1347.

Appendix

A brief operating instruction of wireless sensors is presented in this appendix.

A Implementation of Narada Sensors

It is required to install the Narada data acquisition software (from Civionics website) in a computer as illustrated in Fig. A1(a), to adjust and check the data acquisition of attached sensors. The data acquisition file shown in Fig. A1 (b) includes important specifications that can identify testing properties such as: sampling frequency, time duration, and numbers of sensing units and transducers, where they can be customized as desired. The approach of implementing Narada system is explained in the following steps:

1. Position the Narada transducers appropriately on desired locations, and attach them to the sensing units to wirelessly communicate with the base station that is connected to a computer within a distance range.
2. Once the software is installed, a list of functions is available to adjust and utilize the Narada sensor as desired.
3. Identify the quantity and serial number of sensing units and transducers in the data acquisition file as well as sampling frequency and time duration.
4. Select option 10 from the list of functions shown in Fig. A1 to start collecting data from the channels. Recording will continue until the pre-determined time ends.
5. Ensure that testing is successfully completed and data observed from each channel is saved in a separate file.

```

*****
*
* Welcome to the Narada wireless data interrogation system
*
*
*           Civionics, LLC
*         University of Michigan
*
*           Version 3.0
*           Copyright 2012
*
*****
Attempting to open Serial Port COM3...
Changing serverID to 0x7856...
Changing panID to 0xCDAB...
Changing Channel to 11...
...successfully opened Serial Port COM3

State: SERVER_READY
Please choose an option from the list:
00: Exit Program
01: Check for current status of one wireless sensor
02: Check for current status of entire wireless network
03: Change radio settings on one unit
07: Change Zigbee channel
08: Reboot a unit remotely
09: Change server-side receiver settings
10: Collect sensor data from network
14: Recollect DAQ data from network

>>

```

(a) Narada software

```

DAQ settings file for Narada system.
Version 2.1
*****
Row 1: Sampling Frequency (in HZ)
- Sampling frequency must be an integer value
- If frequency is equal to or above 20 Hz,
  ideal frequencies will divide into 1,000,000.
- If frequency is below 20 Hz,
  ideal frequencies will divide into 31,250.
*****
200
*****
Row 2: Sampling Time (in Seconds)
- Sampling time must be an integer value
- To sample for an infinite amount of time, enter 0
*****
25
*****
Row 3: Number of samples per polling cycle
*****
30000
*****
Row 4: Number of sensing units used (MAX = 50 for now)
*****
2
*****
Row 5: Sensing unit numbers
- Example: 2 5
- Meaning: Unit No.2 and No.5 are being used.
*****
11 12
*****
Row 6: Total number of DAQ channels for each unit
- Use one line for each unit specified in Row 4
- Four DAQ channels are available for each unit: ch0 - ch3.
- Example: 2      0 2
- Meaning: This unit will use two channels, ch0 and ch2.
*****
4 0 1 2 3
3 0 1 3

```

(b) Data acquisition file

Figure A1: Data acquisition system of Narada sensor

As shown in Fig. A1(b), a sampling frequency of 200 Hz is set to measure data for 25 seconds which results in 5000 samples of data collection. The number of sensing units used for testing must be given in row 4 followed by the serial number of each unit in row 5 (i.e., serial number can be found on the unit). The numbers of transducers and channels used for testing are identified in the last two lines where the sequence of rows corresponds to the sequence of units' serial numbers entered in the file. For example, the last line in Fig. A1 (b) is written to utilize 3 sensing transducers attached to channels 0, 1 and 3 of unit number 12.